Food Hydrocolloids 167 (2025) 111454

Contents lists available at ScienceDirect

Food Hydrocolloids

journal homepage: www.elsevier.com/locate/foodhyd

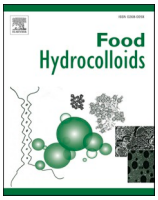

Alginate-pectin microparticles embedding self-assembling antimicrobial peptides and resveratrol for antimicrobial and anti-inflammatory applications

Cesar Augusto Roque-Borda [a,*], Marco Roberto Chávez-Morán [b], Laura Maria Duran Gleriani Primo [c], José C.E. Márquez Montesinos [d,i], Vinicius Martinho Borges Cardoso [c], Mauro M.S. Saraiva [e], Caroline Maria Marcos [c], Marlus Chorilli [c], Fernando Albericio [f,g,**], Beatriz G. de la Torre [h], Fernando Rogério Pavan [c], Andréia Bagliotti Meneguin [c,***]

[a] Vicerrectorado de Investigación, Universidad Católica de Santa María, Arequipa, Peru
[b] Universidad Nacional de Frontera, Facultad de Industrias Alimentarias y Biotecnología, Piura, Peru
[c] São Paulo State University (UNESP), Tuberculosis Research Laboratory, School of Pharmaceutical Sciences, Araraquara, Brazil
[d] Center for Bioinformatics, Simulation and Modeling (CBSM), Universidad de Talca, Talca, 3460000, Chile
[e] São Paulo State University (UNESP), School of Agricultural and Veterinary Sciences, Jaboticabal, SP, Brazil
[f] Peptide Science Laboratory, School of Chemistry and Physics, University of KwaZulu-Natal, Durban, 4001, South Africa
[g] CIBER-BBN, Networking Centre on Bioengineering, Biomaterials and Nanomedicine, and Department of Organic Chemistry, University of Barcelona, 08028, Barcelona, Spain
[h] KRISP, School of Laboratory Medicine and Medical Sciences, College of Health Sciences, University of KwaZulu-Natal, Durban, 4041, South Africa
[i] Center for Nanomedicine, Diagnostics and Drug Development (ND3), Molecular Physiology Laboratory, School of Medicine, University of Talca, Talca, Chile

A R T I C L E I N F O

Keywords:
Antimicrobial peptides
Alginate
Pectin
Controlled release
Self-assembled microstructures

A B S T R A C T

Integrating antimicrobial peptides (AMPs) into alginate-pectin-based microstructured delivery systems enhances the controlled release and stability of bioactive like resveratrol. This study examines spray-dried microparticles utilizing alginate and pectin as primary carbohydrate polymers combined with aggregated AMPs for dual antioxidant and antimicrobial effects. The AMP was self-assembled into nanostructures upon interaction with alginate and pectin, which were subsequently incorporated into spray-dried microparticles, resulting in a stable delivery system. *In silico* modeling and *in vitro* release studies under simulated gastrointestinal conditions showed that AMP-containing microparticles provided a slower, sustained resveratrol release than peptide-free systems. The Weibull model best described the release, indicating a multi-phase behavior driven by diffusion and erosion. In gastric simulated conditions, the alginate-pectin matrices with AMP improved structural integrity, reducing release, while in intestinal ones, partial erosion enabled controlled release. *In vivo* infection studies using *Galleria mellonella* demonstrated significant reductions in inflammation and bacterial load 48 h post-infection. These results suggest that alginate-pectin microparticles with aggregated AMPs enhance the antioxidant release and maintain antimicrobial activity, making them promising for gastrointestinal applications. According to these promising findings, the next step studies will aim to enhance site-specific therapeutic performance through formulation refinement and targeted delivery strategies.

This article is part of a special issue entitled: Boosting structural food science published in Food Hydrocolloids.

* Corresponding author. Vicerrectorado de Investigación, Universidad Católica de Santa María, Arequipa, Peru.
** Corresponding author. CIBER-BBN, Networking Centre on Bioengineering, Biomaterials and Nanomedicine, and Department of Organic Chemistry, University of Barcelona, 08028, Barcelona, Spain.
*** Corresponding author. School of Pharmaceutical Sciences - Sao Paulo State University, Sao Paulo, Brazil.
E-mail addresses: roqueb.cesar@gmail.com, cesar.roque@unesp.br (C.A. Roque-Borda), albericio@ub.edu (F. Albericio), andreia.meneguin@unesp.br (A.B. Meneguin).

https://doi.org/10.1016/j.foodhyd.2025.111454
Received 27 January 2025; Received in revised form 8 April 2025; Accepted 13 April 2025
Available online 15 April 2025
0268-005X/© 2025 The Authors. Published by Elsevier Ltd. This is an open access article under the CC BY license (http://creativecommons.org/licenses/by/4.0/).

1. Introduction

Infectious diseases that cause intestinal inflammation are primarily linked to pathogens such as bacteria, viruses, and parasites able to invade the gastrointestinal tract (Moreira Lopes et al., 2020). Common conditions include infections by *Salmonella enterica, Escherichia coli*, and *Clostridium difficile*, which trigger an immune response, leading to intestinal lining inflammation (Galán, 2021). The body's immune system responds to these infections by releasing pro-inflammatory cytokines, which aim to eliminate the pathogen but at the cost of causing tissue damage (Raheem et al., 2021). Chronic infections or repeated exposure to these pathogens can contribute to more severe conditions, such as inflammatory bowel diseases (IBD), including Crohn's disease and ulcerative colitis (Haneishi et al., 2023; Khor et al., 2011). Effective treatment focuses on eradicating the infection while controlling inflammation to prevent long-term damage to the intestinal mucosa (Higashiyama & Hokaria, 2023).

The gastrointestinal tract is a complex and dynamic system that serves as the first line of defense against external pathogens while facilitating nutrient absorption and immune surveillance (Barajas-Álvarez et al., 2023; Sekirov & Finlay, 2009). Disruptions in intestinal homeostasis are linked to a spectrum of diseases, including IBD, infections, and metabolic disorders (Zhang & Li, 2014). Resveratrol, a polyphenolic compound naturally found in grapes, berries, and peanuts, has been extensively studied due to its antioxidant, anti-inflammatory, and immunomodulatory properties, which make it a promising therapeutic agent for enhancing intestinal defense mechanisms (Huang et al., 2017). However, its clinical application is significantly limited by poor water solubility, rapid metabolic degradation, and low bioavailability, necessitating innovative delivery strategies to realize its full therapeutic potential (Rostami et al., 2019a; Zhang et al., 2019). Resveratrol's mechanism of action involves the modulation of TLR4/NF-κB/NLRP3 signaling pathways, reducing oxidative stress and inflammation at the cellular level (Ding et al., 2023). Its anti-inflammatory effects have been explored in various models of chronic diseases, including arthritis, cardiovascular disease, and IBD. This compound is newsworthy for its therapeutic potential and role in promoting overall health and reducing the risk of inflammation-related conditions (Gowd et al., 2022).

Antimicrobial peptides (AMPs) have emerged as versatile biomolecules due to their intrinsic antimicrobial activity and ability to interact with biological membranes (da Costa de Souza et al., 2022; Polinário et al., 2023). Beyond their role in innate immunity, certain AMPs can self-assemble into well-defined nanostructures and microparticles, offering a novel platform for drug delivery systems (Fichman & Gazit, 2014, pp. 1671–1682). The self-assembly process is driven by a combination of hydrophobic interactions, electrostatic forces, and hydrogen bonding, enabling the formation of stable structures capable of encapsulating therapeutic agents (Levin et al., 2020). Recent studies have demonstrated that AMPs can be rationally designed to form higher-order architectures such as nanofibers, nanoparticles, and hybrid microstructures with tailored functionalities (Wang, Zhang, et al., 2024). These include pH-responsiveness, enzymatic degradation resistance, and the ability to selectively interact with microbial membranes, making them ideal candidates for targeted therapeutic delivery (Deng et al., 2024).

In addition to acting as standalone antimicrobial agents, AMPs have shown potential as co-delivery vehicles in combination therapies with conventional antibiotics or antioxidant molecules, enhancing therapeutic efficacy and reducing the likelihood of resistance (Wang, Wu, et al., 2024). By harnessing the self-assembly properties of AMPs, it is possible to create microparticles that protect resveratrol from enzymatic degradation in the gastrointestinal tract and provide controlled release at the target site. Previous systems utilizing alginate or pectin as carriers have demonstrated variable success in protecting bioactive (Iqbal et al., 2024; Mormile et al., 2024; Song et al., 2024; Yuan et al., 2025; Zheng et al., 2024); however, none have incorporated self-assembling AMPs within alginate-pectin microparticles. This study proposes a novel peptide–polymer formulation, in which self-assembling antimicrobial peptides are incorporated into alginate–pectin microparticles together with resveratrol. The structural integration of these components is hypothesized to contribute to the stability and controlled release of the bioactives, aiming to enhance their therapeutic potential in gastrointestinal applications (Sun et al., 2018).

The self-assembly capabilities of AMPs enable the development of self-assembled peptide–polymer microparticles based on alginate and pectin, enhancing the controlled release of resveratrol while maintaining structural stability in gastrointestinal conditions (Deng et al., 2024). These microparticles are hypothesized to improve local resveratrol bioavailability, provide targeted antimicrobial and anti-inflammatory effects, and offer a promising platform for polysaccharide-based drug delivery systems. This study proposes a multidisciplinary approach combining computational modeling, material science, microbiology, and pharmacological evaluation to design self-assembling peptide–polymer microparticles. These microparticles aim to improve resveratrol protection and enable controlled release under gastrointestinal conditions. The incorporation of AMPs as structural components introduces a biofunctional mechanism that enhances the stability and performance of the delivery platform, offering a promising strategy for the development of next-generation formulations for intestinal applications.

2. Material and methods

2.1. Chemical reagents

Low methoxyl pectin derived from citrus peel (batch SK82079, CP Kelco, Copenhagen, Denmark) was used, with a molecular weight of 170–230 kDa and a degree of esterification of 36.4 %. Lipopolysaccharide from *Escherichia coli* (LPS), 2,2-diphenyl-1-picrylhydrazyl (DPPH) radical and sodium alginate low molecular weight (12,000–40,000 g mol^{-1}, M/G ratio of 0.8) were purchased from Sigma-Aldrich (St. Louis, MO, USA). Fmoc-protected amino acids and Rink Amide MBHA-resin were obtained from AAPPTEC (Louisville, KY, USA), along with reagents such as trifluoroacetic acid (TFA), 4-methylpiperidine (4-MePip), 1-hydroxybenzotriazole hydrate (HOBt), triisopropylsilane (TIS), *N,N′*-diisopropylcarbodiimide (DIC), and acetonitrile. Dimethylformamide (DMF) was sourced from Neon Comercial (São Paulo, Brazil), and dichloromethane (DCM) was purchased from Anidrol Products Laboratories (São Paulo, Brazil). Lysogeny Broth (LB) agar was obtained from Exodo Cientifica (São Paulo, Brazil), and Roswell Park Memorial Institute (RPMI)-1640 medium was acquired from Thermofisher Scientific, Inc (Waltham, MA, USA).

2.2. Antimicrobial peptide synthesis

The 21-residue antimicrobial peptide W^{1}-B1CTcu5C^{15}A, C^{22}S—abbreviated as CR2109 in this work—with the sequence WLIAGLAANFLPQILAKIARKS, was synthesized manually using standard solid-phase peptide synthesis (SPPS) techniques employing the Fmoc/tBu strategy. Initially, the RinkAmide MBHA-resin was washed with a 1:1 (v/v) mixture of DMF and DCM. The removal of the Fmoc group was carried out using a 20 % solution of 4-MePip in DMF. Subsequent Fmoc-amino acids were coupled to the growing peptide chain using 1.2 equivalents of each amino acid and activated with 1.2 equivalents each of HOBt and DIC in DMF/DCM for 2 h at room temperature.

Upon completion of the peptide assembly, the peptide was cleaved from the resin using a cleavage cocktail composed of TFA, TIS, and water in a ratio of 95:2.5:2.5 (v/v/v) for 2 h at RT. The cleaved peptide was precipitated by adding cold diethyl ether and centrifuged at 6500 rpm for 5 min at RT, repeated three times, to remove soluble by-products. The ether supernatant containing hydrophobic impurities was discarded, and the remaining solid peptide/resin was dried under

evaporation to remove residual ether. The dried peptide was then dissolved in a mixture of aqueous solvent A (0.045 % TFA) and acetonitrile solvent B (0.036 % TFA) in a 1:1 (v/v) ratio, followed by centrifugation to separate any insoluble material. The peptide solution was lyophilized using a Liotop lyophilizer (model K108, Brazil). The purity of the peptide was assessed using liquid chromatography as described in the following section.

2.3. AMP characterization

2.3.1. Purification

The purity and identity of synthesized peptide were confirmed using High-Performance Liquid Chromatography (HPLC) and Mass Spectrometry (MS). HPLC analyses were performed on a Shimadzu system equipped with a DGU-20A5R membrane degasser, CTO-20A column oven, SIL-10AF automatic sampler, FRC-10A fraction collector, SPD-20A UV detector, and LC-20AT dual pump. An initial analytical HPLC run was conducted to profile the crude peptide using a reverse-phase C18 column (250 × 4.6 mm, 4.6 μm pore size). The mobile phase consisted of solvent A (0.045 % TFA in water) and solvent B (0.036 % TFA in acetonitrile). A gradient elution was applied, varying solvent B from 5 % to 95 % over 30 min at a flow rate of 1 mL min^{-1}, with detection at 220 nm and 280 nm wavelengths. The column oven was maintained at 40 °C.

Following the peptide's retention time identification, purification was performed using semi-preparative HPLC with a reverse-phase C18 column (250 × 20 mm, 15 μm pore size). The same solvents were used as the mobile phase at a 5 mL min^{-1} flow rate; the gradient program adjusted solvent B from 30 % to 60 % over 90 min at 40 °C. Approximately 60 mg of the peptide was dissolved in 5 mL of a 70:30 (v/v) mixture of solvents A and B and manually injected into the system. Detection was again performed at 220/280 nm. Fractions corresponding to the peptide were collected using the automatic fraction collector. These fractions were re-analyzed under the same analytical HPLC conditions to confirm the purity and identity of the CR2109 peptide. Mass spectrometry analyses were conducted using Liquid Chromatography coupled with Mass Spectrometry (LC-MS) on a Shimadzu UFLC Prominence system interfaced with a Bruker Amazon SL mass spectrometer. The LC-MS was operated under the same conditions as the analytical HPLC, with a reduced flow rate of 0.5 mL min^{-1}. The mass-to-charge ratio (m/z) data confirmed the successful synthesis of the CR2109 AMP.

2.3.2. *In silico* - computational analysis and molecular modeling of the peptide

Before embarking on experimental procedures, it is advantageous to utilize *in silico* tools, such as previously reported (Aronica et al., 2021; Fan et al., 2020; Morena et al., 2024; Roque-Borda et al., 2023). This approach enhances the likelihood of predicting bioactivity and assessing physicochemical parameters, enzyme digestion, and ADMETox (Absorption, Distribution, Metabolism, Excretion, and Toxicity) properties. Various web servers were employed to obtain comprehensive data on peptide CR2109. Furthermore, an in-depth structural bioinformatics analysis was conducted to elucidate the significance of receptor-peptide interactions at the atomic level.

2.3.2.1. Bioactivity, physicochemical features and toxicity prediction. The bioactivity of peptide CR2109 was predicted using the PeptideRanker web server, which applies an N-to-1 Neural Network to estimate bioactivity probability, with scores above 0.5 indicating likely bioactivity (Mooney et al., 2012). AMP activity was further predicted through multiple tools: AI4AMP (deep learning model based on AMP data) (Lin et al., 2021); AMPfun (machine learning methods considering AMP diversity) (Chung et al., 2020), and the tool from CAMPR4 that allows the prediction of the AMP activity applying the Random Forest algorithm (Gawde et al., 2023). Physicochemical properties, including molecular weight, extinction coefficient, isoelectric point, and solubility, were computed using PepCalc (http://pepcalc.com/), accounting for the C-terminus amide group. Toxicity predictions were made using ToxinPred3, an advanced tool combining machine learning and motif analysis for high-accuracy toxicity prediction in peptides of 35 amino acids or fewer (Rathore et al., 2024). Lastly, cell-penetrating peptide activity was computed using a hybrid model of a support vector machine, binary profile of the peptides, and motif information implemented in the CellPPD web service (Gautam et al., 2013, 2015).

2.3.2.2. Enzymatic digestion. PeptideCutter was used to verify if an enzymatic process would occur (Gasteiger et al., 2005). This was achieved by setting a threshold of cleavage probability at 60 %, simulating the activity of gastrointestinal tract enzymes (chymotrypsin, trypsin, and pepsin).

2.3.2.3. ADMET analysis. The simplified molecular input line entry system (SMILES) format for the CR2109 peptide was generated using the PepSMI online tool from NovoPro Bioscience Inc. (available at https://www.novoprolabs.com/tools/convert-peptide-to-smiles-string). After adjusting the SMILES string to include the C-terminal amide group, it was visually inspected using the Smi2Depict tool (accessible at http://cdb.ics.uci.edu/cgibin/Smi2DepictWeb.py#). The modified SMILES string was then entered into the ADMET-AI web server to predict its pharmacokinetic and pharmacodynamic properties (Swanson et al., 2024).

2.3.2.4. Protein-peptide molecular docking. Experimentally resolved structures of relevant bacterial target proteins were retrieved from the Protein Data Bank (PDB) (http://www.rcsb.org) (Berman, 2000). The secondary structure of the CR2109 peptide was modeled using the PEP-FOLD4 web server at pH 7, running 100 simulations with 3000 Monte Carlo steps. The best model was selected based on the sOPEP energy score provided by PEP-FOLD4 at pH 7 (Rey et al., 2023). The target proteins and the CR2109 peptide underwent pre-docking structure preparation using the Dock Prep module (Lang et al., 2009; Moustakas et al., 2006) available in the UCSF Chimera suite (Pettersen et al., 2004), where crystallographic water and non-protein molecules were removed, and side chains were completed. Subsequently, molecular docking was performed using the LightDock software (Jiménez-García et al., 2018; Roel-Touris et al., 2020a, 2020b), which employs the Glowworm Swarm Optimization algorithm to dock protein-protein, protein-peptide, and protein-DNA systems (Krishnanand & Ghose, 2009). Docking parameters were adjusted according to the authors' recommendations, with energy calculations based on the DFIRE scoring function (Liu et al., 2004). Then, a post-docking process took place. The docking results refinement was performed with the HADDOCK2.4 web server (Honorato et al., 2021, 2024), taking into account the active residues at 5A of CR2109 in the previous phase. Additionally, the best pose of the refinement was subjected to an MM-GBSA computation using the HawkDock web server (Chen et al., 2016; Hou et al., 2011; Sun et al., 2014; Weng, Wang, Wang, et al., 2019) to obtain more reliable binding affinity values. The molecular docking results were visualized using the PyMOL Molecular Graphics System, Version 2.0 Schrödinger, LLC (Adasme et al., 2021).

2.4. Microencapsulation of resveratrol by spray-drying

2.4.1. Preparation of biopolymer solutions

To prepare the peptide–biopolymer preformulating, alginate and pectin were separately dissolved in distilled water at a concentration of 10 mg/mL. Each solution was stirred for 2 h at room temperature using a magnetic stirrer at 400 rpm to ensure complete dissolution. After the stirring period, the alginate and pectin solutions were combined in a 1:1 ratio by volume to form a homogeneous dispersed phase. This combined solution served as the base for all further formulations.

2.4.2. Addition of resveratrol and peptide CR2109

Following the preparation of the dispersed alginate-pectin phase, resveratrol and/or peptide CR2109 were incorporated depending on the formulation described in Table 1. Resveratrol was first dissolved in a 1:1 methanol-water solution to ensure proper solubilization, followed by homogenization using an Ultra-Turrax disperser. Separately, peptide CR2109 was dissolved in a phosphate buffer solution (0.1 M; pH 7.4) to maintain stability and charge distribution. The complete mixture was then stirred for 20 min at room temperature using a mechanical stirrer (IKA Eurostar 60 Digital, IKA®-Werke GmbH & Co. KG, Germany) at 1350 rpm before the spray drying processing.

Upon addition to the anionic alginate–pectin matrix, the cationic CR2109 peptide underwent spontaneous self-assembly driven by dual electrostatic and hydrophobic interactions, leading to the formation of peptide–polymer complexes. To monitor this process, the Zeta potential of the solution was measured immediately using a dynamic light scattering and Zeta potential analyzer (Malvern Zetasizer Nano ZS, Malvern Instruments Ltd., UK). A significant shift in Zeta potential values indicated the successful formation of nanoassemblies, suggesting that CR2109 was uniformly dispersed and stably integrated within the polymeric solution. However, it is important to note that while Zeta potential readings and changes in PDI suggested nanoparticle formation, this method alone is insufficient to characterize nanoassemblies definitively. To support this observation, complementary analyses such as scanning electron microscopy (SEM) and particle size distribution (Table 2) were used to strengthen the evidence for self-assembly and nano-in-micro structure formation. After confirmation of AMP nanoassemblies via Zeta potential, the solution underwent immediate spray drying to yield the nano-in-micro structured microparticles.

2.4.3. Microencapsulation by spray dryer

Microparticles were prepared using a laboratory-scale spray dryer (Mini Spray Dryer B-191, BUCHI, Switzerland) according to Lopes et al., (Lopes et al., 2025). This compact system features a borosilicate glass drying chamber and cyclone, with overall dimensions of 500 × 1000 × 600 mm (l × h × d). The unit includes a peristaltic pump for solution feed and a pneumatic spray nozzle with a 0.7 mm diameter orifice. Before spray drying, operational parameters were set: inlet temperature at 145 °C, outlet temperature at 67 °C, aspirator at 70 %, pump rate at 5 %, airflow at 600 L/h, and atomization pressure at 5 bar. The formulation yield (%) was calculated to assess the efficiency of microparticle recovery after the spray drying process. This parameter was determined by comparing the mass of the dry microparticles collected with the total mass of solids (biopolymers and active compounds) initially used in each formulation. Solvent volumes were not included in this calculation, as they were completely evaporated during spray drying. The yield was calculated using the following equation:

$$Yield\ (\%) = \frac{Mass\ of\ recovered\ microparticles\ (mg)}{Total\ initial\ mass\ of\ solids\ (mg)} \times 100 \qquad \text{Eq. (1)}$$

2.5. Characterization of formulated microparticles

2.5.1. Physicochemical and morphological characterization

The FT-IR spectra of the formulated microparticles were obtained using a PerkinElmer Frontier spectrometer with an attenuated total reflectance (ATR) accessory (Bruker Vertex 70 FTIR). The transmittance spectra were recorded with a resolution of 4 cm^{-1}, covering a wavenumber from 4000 to 400 cm^{-1}. Data analysis was performed using OriginPro 2019b software. The surface morphology of the formulated microparticles was examined using a field emission scanning electron microscope (FE-SEM) (Jeol Ltd., Japan). Samples were carbon-coated and mounted on stubs using adhesive tape. Imaging of the surface and cross-sections was conducted at 2.0 kV with a 10 μA current, a working distance of 6.5 mm, and secondary electron mode at 5000 × magnification. Thermal stability was evaluated through thermogravimetric analysis (TGA), differential scanning calorimetry (DSC), and derivative thermogravimetry (DTG). Approximately 10–12 mg of each sample (including microparticles, pure peptide, and empty microparticles) were placed in alumina crucibles. The analyses were conducted under a synthetic air flow (100 mL/min) over a temperature range of 30–600 °C, with a heating rate of 5 °C/min. The data were collected using a DSC-TGA instrument (SDT Q600 V20.9 Build 20, TA Instruments) and processed using Universal Analysis 2000 software.

Table 1
Composition of the formulated microparticles containing self-assembled peptides and resveratrol, data expressed in mg per 100 mL.

Sample	Blank	ALG/P@Resv	ALG/P@AMP	ALG/P@Resv/AMP
Pectin	1000	1000	1000	1000
Alginate	1000	1000	1000	1000
CR2109	0	0	3.2	3.2
Resveratrol	0	100	0	100

2.6. In vitro studies

2.6.1. Drug content and in vitro release

The drug content (DC) was determined by dispersing 15 mg of the peptide/resveratrol-loaded samples in 3 mL of phosphate buffer solution (0.1 M; pH 7.4), based on the drug solubilities. The mixture was stirred magnetically at 750 rpm for 16 h, followed by a 40 min incubation in an ultrasonic bath. Afterward, the samples were centrifuged at 5000×*g* for 10 min, and the supernatant was filtered using 0.45 μm nylon membranes. The encapsulation efficiency (EE%) was determined by dispersing 5 mg of the spray-dried microparticles in 6 mL of phosphate buffer solution (0.2 M; pH 7.4) according to Sales et al., (Sales et al., 2023). The dispersion was magnetically stirred at room temperature until complete solubilization. The samples were then centrifuged at 3000×*g* for 10 min, and the resulting supernatant was filtered through a 0.45 μm nylon membrane to remove any undissolved particles or excipients.

Resveratrol content was quantified using a UV–vis spectrophotometer (Hewlett Packard-Kayak XA) at 306 nm, while peptide content was assessed using a fluorescence-based method with fluorescamine. In a 96-well microtiter plate, 90 μL of the supernatant was mixed with 10 μL of fluorescamine solution (5 mg/mL in acetone). The samples were prepared in triplicate to ensure reproducibility. After mixing, the plate was incubated for 5 min at 37 °C to optimize the reaction between fluorescamine and the free amino (NH_2) groups on the peptide surface. The resulting fluorescence was measured using an excitation wavelength of 360 nm and an emission wavelength of 465 nm, as described by Tenland et al. (Tenland et al., 2019). The drug content and encapsulation efficiency were calculated using the following equations:

$$DC\ (\%) = \frac{Amount\ of\ encapsulated\ compound}{Total\ mass\ of\ microparticles} \times 100 \qquad \text{Eq. (2)}$$

$$EE\ (\%) = \frac{Amount\ of\ encapsulated\ drug}{Amount\ of\ drug\ initially\ added} \times 100 \qquad \text{Eq. (3)}$$

The gastrointestinal tract (GIT) environment was simulated by immersing 10 mg of microparticles in 10 mL of simulated gastric fluid (SGF) and simulated intestinal fluid (SIF). SGF was prepared with 0.1 mol/L HCl at pH ≈ 2, while SIF was prepared using Sorensen's phosphate buffer at pH 7.4 (Anbinder et al., 2011). Samples were taken at different time intervals (5, 10, 20, 40, 60, 120, and 180 min) and quantified using the same method applied for drug content calculation, measuring absorbance at 280 nm. For resveratrol, quantification was performed by UV at 306 nm and for peptide release, the fluorescamine method was used as described above. Each procedure was performed at least 3 times.

Table 2
Characteristics of nano-in-microparticles formed with peptide and resveratrol.

System/dispersion	EE (%)		DC (%)		Yield (%)	PDI	Zeta potential (mV)	Size (nm)
	Resv	AMP	Resv	AMP				
Blank	–	–	–	–	33.22	0.552	−25.0	894.5
ALG/P@Resv	78.21	–	39.10	–	40.87	0.456	−17.5	362.7
ALG/P@AMP	–	66.39	–	0.259	14.44	0.364	−7.4	220.6
ALG/P@Resv/AMP	76.11	72.84	89.23	2.73	4.06	0.185	−18.2	152.8
AMP	–	–	–	–	–	0.338	+10.6	–
Resv	–	–	–	–	–	0.570	−5.8	880.2

EE: encapsulation efficiency. DC: drug content. Resv: resveratrol. AMP: CR2109 antimicrobial peptide.

2.6.2. Mathematical modeling of release kinetics

To describe the resveratrol release behavior from the microparticles, various mathematical models were applied to the experimental data, including Baker-Lonsdale, Higuchi, Korsmeyer-Peppas, First-order, Hixson-Crowell, and Weibull models.

Baker-Lonsdale Model: The Baker-Lonsdale model was used to describe diffusion-controlled release from spherical matrices, with equation (4):

$$F(t) = \frac{3}{2}\left[1 - \left(1 - \frac{Mt}{M\infty}\right)^{2/3}\right] - \frac{1}{2}\frac{Mt}{M\infty} \quad \text{Eq. (4)}$$

Where *Mt*is the amount of drug released at time *t*, and *M*∞ is the total amount of drug released at infinite time.

Higuchi Model: The Higuchi model assumes a diffusion-based release mechanism and is represented by equation (5):

$$Mt = k \cdot t^{1/2} \quad \text{Eq. (5)}$$

Where *Mt*is the amount of drug released at time *t* and *k* is the diffusion rate constant.

Korsmeyer-Peppas Model: This model was applied to analyze the release mechanism when the release does not follow Fickian diffusion. equation (6) is:

$$Mt \ / \ M\infty = k \cdot t^{n} \quad \text{Eq. (6)}$$

Where Mt/M∞ is the fraction of drug released at time *t*, *k* is the kinetic constant, and *n* is the release exponent, which indicates the mechanism of release (Fickian diffusion if $n < 0.45$, non-Fickian transport for $0.45 < n < 0.89$).

First-order Kinetics: First-order kinetics assumes that the release rate is proportional to the concentration of the drug remaining in the microparticles. The model is represented by equation (7):

$$\ln\left(1 - \frac{Mt}{M\infty}\right) = k \cdot t^{n} \quad \text{Eq. (7)}$$

where *k* is the release rate constant.

Hixson-Crowell Model: The Hixson-Crowell model was used to evaluate systems where there is a change in surface area and diameter during dissolution. It is described by Eq. (8):

$$\left(M_0^{1/3} - M_t^{1/3}\right) = k \cdot t \quad \text{Eq. (8)}$$

where M_0 is the initial mass of the drug, and M_t is the remaining mass at time *t*.

Weibull Model: The Weibull model was applied to describe the complex release profile and is given by equation (9):

$$F(t) = 1 - e^{-(t/\tau)^{\beta}} \quad \text{Eq. (9)}$$

where $F(t)$ is the fraction of drug released at time *t*, τ is the time constant, and β is the shape parameter that provides insights into the release mechanism (diffusion-controlled for $\beta < 1$, case-II transport for $\beta = 1$, and complex release for $\beta > 1$).

2.6.3. Antioxidant activity by DPPH assay

The antioxidant capacity of the formulated microparticles was determined using a modified version of the DPPH radical scavenging assay, based on the methodology of Deladino et al. (Deladino et al., 2008). Methanol was chosen as the solvent after previous testing showing no significant variation compared to other solvents. A stock solution of 25 mg/L DPPH• in methanol was prepared, and its absorption spectrum was measured to identify the wavelength of maximum absorbance. Each sample received 100 μL of this solution, diluted to a total volume of 3.9 mL with the DPPH•-methanol mixture. Absorbance measurements were taken at 520 nm periodically, reaching stability after 2 h. The percentage of DPPH• inhibition was calculated using equation (10), allowing for the evaluation of the microparticles' antioxidant activity and their potential as radical scavengers by percentage of inhibition (%).

$$I\% = \left[\frac{DPPH\ absorbance - Sample\ absorbance}{DPPH\ absorbance}\right] x100 \quad \text{Eq. (10)}$$

2.6.4. Antibacterial activity assays

The antimicrobial susceptibility of CR2109 peptide was evaluated using the Minimum Inhibitory Concentration (MIC) test with the broth microdilution technique following the Clinical Laboratory Standards Institute (CLSI) (C. L. S. I. P, 2018). The test was performed using the field strains: *E. coli* ($bla_{CTX\text{-}M\text{-}2}$; *mcr-1*); *S.* Minnesota (*aac(6′)-Iaa*; $bla_{OXA\text{-}129}$; *qnrB19*), and *Klebsiella pneumoniae* (*aadA1b*; $bla_{TEM\text{-}1}$; *dfrA1*; *strAB*; *sul2*; *tetA*); *K. pneumoniae* ($bla_{NDM\text{-}1}$) sampled from swine, poultry, and goat, respectively. Additionally, the standardized strains *E. coli* C600 (Allué-Guardia et al., 2019), *S.* Mbandaka SAMN37152292 (p109518) (Benevides et al., 2024), and *S.* Typhimurium F98 (pH2332-107) (Barrow et al., 1990). *E. coli* ATCC 25922 was used as a quality control strain.

2.6.5. Cell viability

Cytotoxicity was assessed in J774A.1 macrophage (ATCC® Tib-67™, 8 passages) using the resazurin-based cell viability assay (AlamarBlue®) following the methodology of Primo et al. (Primo et al., 2024). Cells were initially cultured in RPMI media supplemented with 10 % fetal bovine serum, along with gentamicin (75 μg/mL) and amphotericin B (3 μg/mL), under standard conditions (5 % CO_2, 37 °C). To determine the IC_{50}, cells (2.5×10^5 cells/mL in RPMI) were plated in 96-well plates and incubated for 24 h under the same conditions. After incubation, cells were exposed to 3.2 % samples prepared in phosphate-buffered saline (PBS, pH 7.4, 1:9 v/v) for another 8 h, followed by quantification through fluorescence intensity.

2.7. In vivo studies

2.7.1. Toxicity assessment in Galleria mellonella

As *Galleria mellonella* (*G. mellonella*) is an invertebrate, no ethics committee approval was required for the study. The toxicity of the microparticles was evaluated on *G. mellonella* larvae based on the method outlined by Emery et al. (Emery et al., 2019). The larvae were injected in the pro-leg with 10 μL of sample suspensions at 10 mg/mL and 500

μg/mL concentrations. Survival rates were recorded, and the health of the larvae was monitored daily over five days.

2.7.2. Inflammation and infection in Galleria mellonella

Inflammation was initiated by administering a 0.2 μg/μL dose of LPS via injection. For infection, 5 μL of a bacterial suspension with 10^2 colony-forming units (CFU)) was injected. After a 4-h incubation period post-infection, the larvae were treated with the microparticle formulation, which had been suspended in PBS. Following 24 h of treatment, larvae hemolymph was extracted and plated onto LB Agar to quantify bacterial burden. CFU counts were performed daily to monitor infection progression and treatment efficacy (detection limit was $<10^2$ CFUs).

For histological examination, treated and control larvae were fixed by injecting 10 μL of 4 % paraformaldehyde into the last left pro-leg using an insulin syringe, following the procedure by Meneguin et al., (Meneguin et al., 2024). Afterward, the samples were placed in cassettes and immersed in 4 % paraformaldehyde for 48 h at room temperature, followed by a 4-h rinse with running water. Sections were stained with hematoxylin and eosin (H&E) for histopathological analysis, and images were captured using a Leica DM2500 optical microscope with a digital camera at 50 × magnification under standardized settings.

2.8. Statistical analysis

All release experiments were performed in triplicate, and the average values were used for mathematical modeling. Correlation coefficients (r^2), for each model, were calculated to determine the best fit to the experimental data. The models with the highest r^2 values were those to best describe the release kinetics for each system in both gastric and intestinal environments. Data were analyzed using GraphPad Prism 9.0 (GraphPad Software, San Diego, CA, USA). Model fitting and regression analysis were performed to extract the kinetic constants for each model. Statistical comparisons were conducted using ANOVA, and a *p*-value of less than 0.05 was considered significant.

3. Results and discussions

3.1. CR2109 AMP has a putative biological effect

The peptide was prepared by SPPS using a very low excess of Fmoc-amino acids (1.2 eq) and 4-MePip instead of piperidine, which is a restricted substance, trying to green the process (Al Musaimi et al., 2020), and characterized by LC/MS, confirming a purity above 95 %. Mass spectrometry peaks at 599.39 (Z = +4), 798.84 (Z = +3), and 1197.77 (Z = +2) correspond to the expected mass-to-charge ratios for a molecule with a molecular weight of 2393 g/mol, matching the theoretical weight of CR2109 and confirming successful synthesis (Fig. S1). *In silico* studies (Table S1) further confirmed an extinction coefficient of 5690 $M^{-1}cm^{-1}$, and a net charge of +4 at pH 7. PeptideRanker predicted a 0.77 probability of CR2109 being bioactive, with high scores across AMP models, suggesting strong antimicrobial potential. Additionally, predictions indicated moderate probabilities for activity against both Gram-negative and Gram-positive bacteria, along with modest likelihoods for antifungal, mammalian cell-targeting, and anticancer activities. Toxicity analysis showed a low likelihood of CR2109 acting as a toxin, despite some potential for targeting mammalian cells.

Enzymatic digestion of CR2109 was simulated *in silico* using the stomach enzyme pepsin (EC 3.4.23.1). The PeptideCutter simulation at pH 1.3 or higher predicts that pepsin (Table S2) will cleave CR2109 at eight sites (positions 1, 2, 5, 6, 9, 11, 14, and 15) with a probability greater than 60 %. Further simulations with pancreatic enzymes chymotrypsin (EC 3.4.21.1) and trypsin (EC 3.4.21.4) indicated that chymotrypsin cleaves at positions 1 and 10 with probabilities of 87.1 % and 67.8 %, respectively, whereas trypsin cleaves at positions 17, 20, and 21 with probabilities of 100 %, 95.3 %, and 83.4 %, respectively. These *in silico* predictions suggest that peptide CR2109 may be susceptible to cleavage in the digestive system, highlighting the need for protective treatments to prevent degradation.

SMILE format for CR2109 was obtained (Table S3), ensuring the presence of the C-terminus amide group. The ADMET profile of peptide CR2109 (Table S4) reveals key insights into its physicochemical properties, absorption potential, metabolism, excretion, and toxicity. With a molecular weight of 2393.96 g/mol, CR2109 falls within the 99.73rd percentile, categorizing it as a large molecule, which poses challenges for membrane permeability and drug-likeness. This is further evidenced by the low LogP value of −4.84 (5.58 percentile), indicating significant hydrophilicity, and the high number of hydrogen bond donors (31) and acceptors (29). Moreover, its Quantitative Estimate of Druglikeness score of 0.01 and Topological Polar Surface Area of 907.56 $Å^2$ underscore the peptide's poor conformity to traditional small-molecule drug design principles, likely limiting passive diffusion through biological membranes.

CR2109's absorption profile indicates low intestinal absorption (17.33 percentile) and poor oral bioavailability (5.27 percentile), aligning with its poor cell permeability. However, the peptide's P-glycoprotein inhibition prediction (70.96 percentile) suggests the potential to circumvent determined efflux mechanisms, though the overall absorption limitations remain significant. In terms of distribution, the peptide shows low potential for blood-brain barrier penetration (4.96 percentile) but moderate plasma protein binding (62.96 %), suggesting that, while not CNS-penetrant, the peptide could maintain a reasonable presence in the systemic circulation, though free drug concentration may be reduced. The metabolism profile indicates that CR2109 is a substrate for CYP3A4 (94.53 percentile), suggesting it may undergo significant hepatic metabolism, potentially reducing its bioavailability. However, its inhibition of other cytochrome P450 enzymes is relatively low, minimizing the risk of broad metabolic interactions. The excretion profile predicts a short half-life of 0.75 h and high microsomal clearance (94.49 percentile), consistent with its rapid metabolism. Importantly, the toxicity analysis highlights a moderate risk for hERG blocking (69.45 percentile), raising some concerns about potential cardiotoxicity, though the overall clinical toxicity, mutagenicity, and carcinogenicity risks are low. These findings suggest that while CR2109 presents challenges for oral administration and systemic absorption, its low toxicity profile and potential antimicrobial activity may make it suitable for targeted delivery systems or localized therapeutic applications.

The results from each PEP-FOLD4 simulation explored different regions of conformational space, clustering similar structures and identifying the top five conformational clusters. Each cluster contains a representative structure, or "best model," with the lowest sOPEP energy value. In this case, all models had energy values around −57, with the lowest being −57.5544 in model 1. As shown in Fig. S2, the structures of the models are nearly identical. Additionally, CR2109 features of net positive charge, distribution of charged and uncharged residues and the amphipathic nature of the structure (middle and bottom of Fig. S2) satisfy the assumption for an AMP that can interact with cell membranes due to its negative charge (Sato & Feix, 2006; Wang et al., 2017; Zhang & Gallo, 2016).

To evaluate the potential of CR2109 to bind relevant bacterial targets after putative membrane disruption, molecular docking was performed using LightDock and its implementation of DFIRE function score, which strongly correlates with theoretical and experimental binding affinities (Zhang et al., 2005), allowed the identification of possible binding poses of CR2109 with the relevant targets (Table S5). Then, the three refinement steps proposed by HADDOCK protocol for refinement were made, avoiding steric clashes observed in the initial docking process with LightDock (Table S5) (Saponaro et al., 2020). Finally, Fig. 1 shows the MM-GBSA computation values by HawKDock implementation after refinement. The MM-GBSA value, which is more accurately related to the binding affinity of a complex than the docking score function, efficiently identifies relevant poses without demanding extensive computational resources (Chen et al., 2016; Weng, Wang, Chen, et al., 2019).

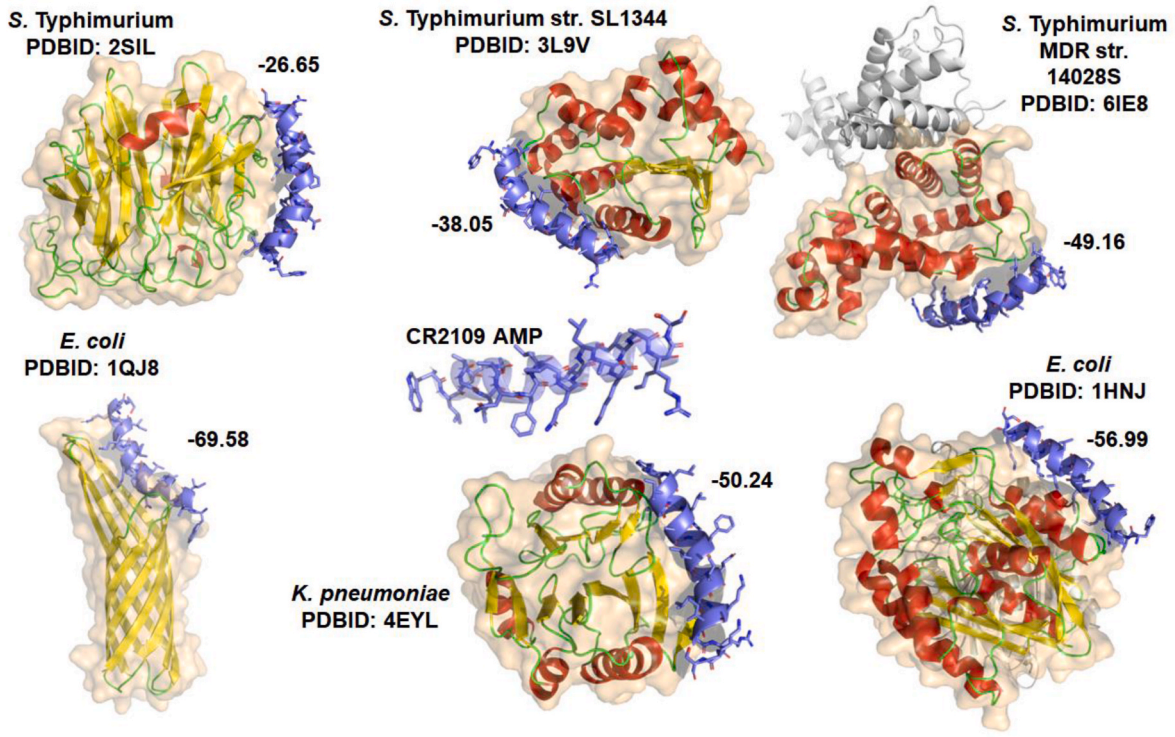

Fig. 1. Target-CR2109 docking results. The binding pose for CR2109 is displayed in purple represented by sticks. The surface of the targets, alpha-helix, beta-sheet and coils are represented in light orange, red, yellow and green, respectively in a cartoon style. Numbers represent the MM-PBSA values in Kcal/mol. (For interpretation of the references to colour in this figure legend, the reader is referred to the Web version of this article.)

In summary, the analysis of the CR2109 peptide reveals several key insights into its behavior in various hostile environments and its ability to exert activity. The results indicate that the peptide can be significantly degraded by present enzymes in the gastric tract, while its degradation is much less pronounced in the intestinal tract. The peptide has the ability to interact with several bacterial membrane and cytoplasmic receptors, allowing it to employ multiple mechanisms of action. According to predictions, it can also cross cellular barriers to exert antimicrobial activity within mammalian cells, thereby preventing systemic infection (Roque-Borda et al., 2022).

3.2. Formulated microparticles with CR2109 are stable at different and defined

Initially, the addition of the antimicrobial peptide CR2109 resulted in significant changes in both zeta potential and polydispersity index (PDI), indicating the formation of self-assembled structures and following the formation of microparticles through spray drying, these parameters were further altered significantly (Table 2). AMP CR2109 was expected to spontaneously self-assemble into nanoparticles via electrostatic interactions and hydrophobic forces upon mixing with negatively charged alginate and pectin, confirmed by a significant shift in Zeta potential indicative of nanoparticle formation (Ochbaum & Bitton, 2017; Wen et al., 2022). This suggests that the microsystem contains peptide-based nanoassemblies, which are likely associated with enhanced stability and controlled release of resveratrol, as demonstrated in the subsequent results.

FTIR analysis was conducted to characterize functional group vibrations between the components of the microparticles (alginate, pectin, resveratrol, and CR2109) and evaluate possible interactions indicating their integration within the matrix. The FTIR spectra of the different formulations are presented in Fig. 2A. The spectra reveal the characteristic bands of the biopolymers alginate and pectin, as shifts and intensity changes possibly induced by the presence of resveratrol and CR2109. The spectrum of the control sample (Blank) shows typical bands corresponding to the functional groups of alginate and pectin, with prominent peaks around ~3300 cm^{-1} (stretching vibrations of -OH groups), ~1600 cm^{-1} (asymmetric stretching of $-COO^-$ groups), and ~1400 cm^{-1} (symmetric stretching of $-COO^-$). These observations are consistent with previous studies reporting the same characteristics for alginate and pectin in aqueous solutions (Costa & Dias, 2021; Mancer & Daoud, 2021).

Formulations containing resveratrol (ALG/P@Resv and ALG/P@Resv/AMP) show an increase in the intensity of the bands near ~1200-1000 cm^{-1}, attributed to the phenolic vibrations of resveratrol (Jeong et al., 2016). These changes may suggest interactions between resveratrol and the biopolymers, likely through hydrogen bonding with the alginate and pectin hydroxyl groups. Previous studies have reported that resveratrol can interact with polymeric matrices through hydrogen bonds, enhancing its stability within encapsulated formulations (Chen et al., 2020; Davidov-Pardo & McClements, 2014; Wegiel et al., 2013). Additionally, a slight shift in the bands around ~1600 cm^{-1} in these formulations indicates potential electrostatic interactions between the negatively charged carboxylate groups of alginates and the positively charged amino groups of the CR2109 peptide (Mirtič et al., 2018). Formulations containing peptide CR2109 (ALG/P@AMP and ALG/P@Resv/AMP) exhibit shifts in the bands around ~3300 cm^{-1} and ~1600 cm^{-1}, which could be attributed to interactions between the amide groups of the peptide and the carboxylate groups of the polymer matrix (Bélanger et al., 2009). This is consistent with the formation of complexes through electrostatic and potentially hydrophobic interactions, which have been reported in studies of peptide encapsulation in alginate matrices (Hole et al., 2005; Trovatti et al., 2018). The presence of the peptide modifies the polymer matrix, creating a favorable environment for the nanoassemblies formed stabilization, which is crucial for maintaining its antimicrobial activity in gastrointestinal applications (Qi et al., 2018; Wang et al., 2021a, 2021b).

The combined formulation (ALG/P@Resv/AMP) exhibits greater

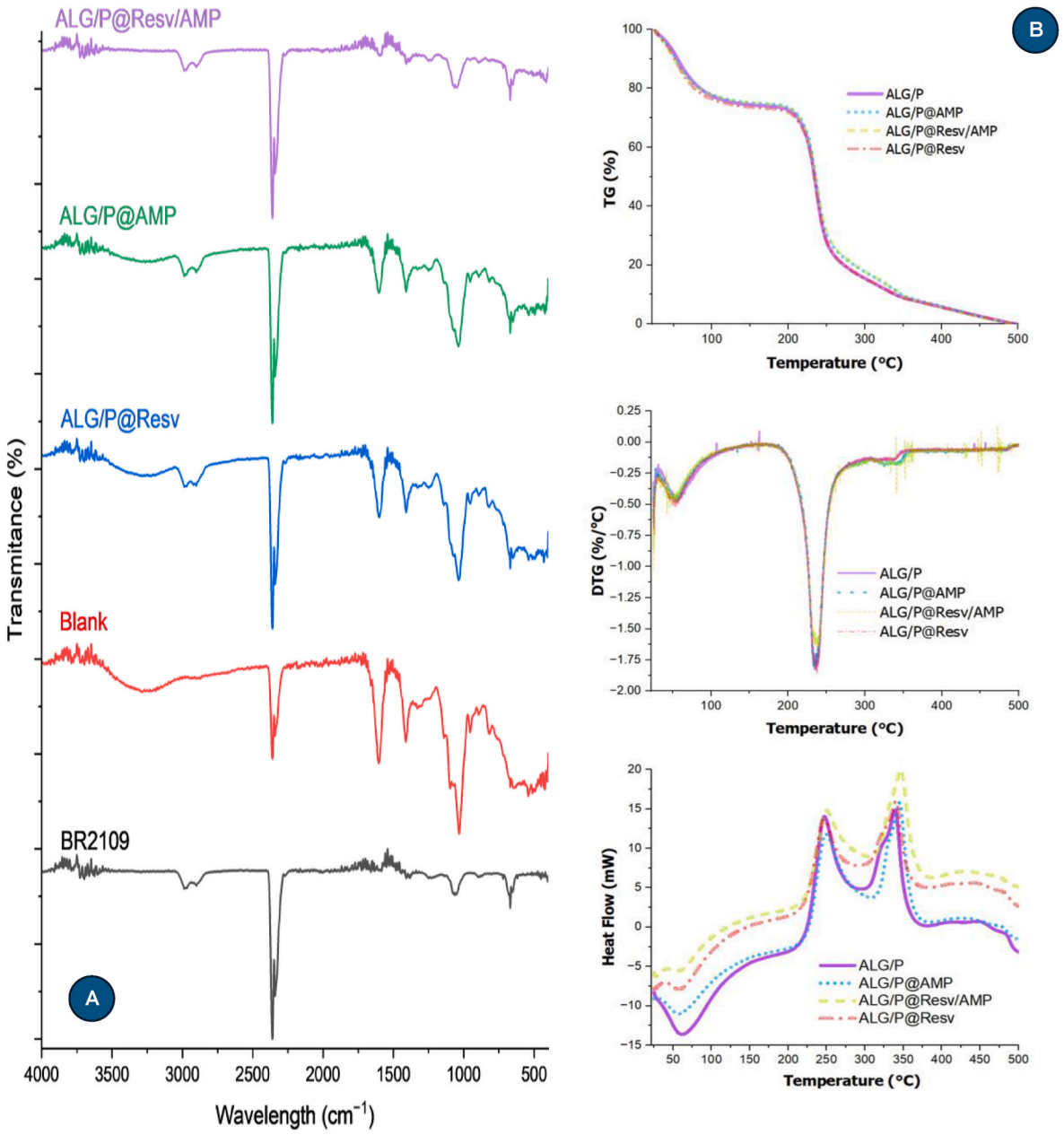

Fig. 2. (A) FTIR spectra of different formulations. The spectra illustrate the characteristic functional groups of alginate and pectin, as well as shifts corresponding to interactions with resveratrol and peptide CR2109. (B) Thermal analysis of the formulations through TGA, DSC, and DTG.

complexity in the spectra within the ~1600-1000 cm^{-1} region, suggesting additional interactions between the peptide and resveratrol within the polymeric matrix (Wang, Yang, et al., 2024). These interactions may result from hydrogen bonding and van der Waals forces that stabilize the microparticle structure, as observed in similar systems for the encapsulation of bioactive compounds (Lengyel et al., 2019). Moreover, the shift in absorbance bands suggests their incorporation and possible influence on the matrix structure, which may contribute to controlled and sustained release. The resveratrol and CR2109 presences in the same matrix provide dual bioactivity, which could be further investigated for possible synergistic effects.

On the other hand, the thermograms presented in Fig. 2B illustrate distinct thermal events and degradation patterns for each formulation, highlighting the effects of encapsulating resveratrol and CR2109. This initial weight loss (50–150 °C) is attributed to the evaporation of residual moisture and volatile components (Bodbodak et al., 2024). The presence of water molecules adsorbed within the matrix is consistent with other studies on biopolymer-based systems, where such events occur at low temperatures (Chen et al., 2008). A more pronounced weight loss is observed (200–300 °C), corresponding to the thermal degradation of the alginate and pectin matrix and this stage indicates the primary degradation of the polymer backbone, crucial for understanding the structural integrity of the microparticles (Chen & Zhang, 2019; Marangoni Júnior et al., 2022; Stachowiak et al., 2021). In formulations containing resveratrol and peptide CR2109, an additional weight loss phase occurs (300–400 °C), indicating the degradation of the encapsulated bioactives. Notably, the temperatures observed for this degradation phase are higher than those for the free compounds, suggesting that the encapsulation process provides thermal protection (Chen et al., 2024; Rostami et al., 2019b; Xun et al., 2023).

Endothermic peaks (50–150 °C) in this region correlate with the evaporation of water, confirming the moisture loss observed in the TGA results and this event is consistent across all formulations, suggesting that the moisture content is similar regardless of the presence of

resveratrol or CR2109 (Bergonzi et al., 2020). The exothermic transitions in this range (200–300 °C) are associated with the decomposition of the alginate-pectin matrix and variations in the intensity and shape of these peaks among different formulations suggest that the incorporation of resveratrol and CR2109 modifies the thermal behavior of the biopolymers (Flamminii et al., 2021). Such modifications may be due to interactions between the biopolymers and the bioactives, possibly involving hydrogen bonding and electrostatic interactions, which have been documented in similar encapsulation systems (Pan et al., 2021). Formulations containing resveratrol and CR2109 (ALG/P@Resv/AMP) exhibit improved thermal stability compared to those with only one active ingredient. This suggests a synergistic effect between the compounds and the biopolymers, likely enhancing the matrix's thermal resistance.

The SEM images (Fig. 3) reveal distinct differences in the morphology and distribution of the microparticles across the various formulations. The blank formulation exhibits densely aggregated and irregular microparticles with undefined contours and rough surfaces, reflecting uncontrolled drying behavior. In contrast, ALG/P@Resv microparticles appear more spherical and dispersed, although surface roughness remains evident, possibly due to the surface deposition of resveratrol.

The ALG/P@AMP microparticles present a heterogeneous distribution of sizes, including large agglomerates and fragmented structures. Their surfaces are rough and porous, suggesting that the antimicrobial peptide presence interferes with the matrix homogeneity and stability during spray drying (Bazán et al., 2023; Belščak-Cvitanović et al., 2015). Interestingly, the dual-loaded ALG/P@Resv/AMP microparticles show the most regular spherical shapes and smoother surfaces in comparison to the AMP-only formulation. The co-encapsulation seems to mitigate the aggregation and roughness caused by the peptide alone, possibly due to balanced intermolecular interactions between resveratrol, peptide, and the biopolymeric matrix. (Manjili et al., 2024).

The surface morphology and sphericity of spray-dried microparticles are known to influence their physicochemical behavior, particularly in terms of hydration, swelling, and release kinetics. The smoother and more compact structure observed in the dual-loaded ALG/P@Resv/AMP formulation may favor a slower diffusion of water and, consequently, a more controlled release of the encapsulated compounds. In contrast, the rougher surfaces and irregular shapes seen in the AMP-only formulation could increase surface area exposure, potentially accelerating initial release or leading to structural instability under gastrointestinal conditions. These morphological features may also impact storage stability by affecting moisture absorption and oxidative degradation, as previously reported in biopolymer-based systems. The morphological heterogeneity observed in the AMP-containing formulations could be attributed to the amphipathic nature and positive charge of the CR2109 peptide, which may interfere with the polymer network formation during the atomization and drying process. Electrostatic repulsion between peptide molecules and ionic interactions with the carboxylate groups of alginate and pectin may result in localized structural perturbations, altering droplet drying dynamics. Similar effects have been described in systems incorporating charged bioactives or proteins into polysaccharide matrices, where surface tension changes or phase separation during spray drying lead to structural defects or aggregation. Therefore, the more homogeneous morphology obtained in the resveratrol–AMP co-formulation may reflect a stabilizing effect of resveratrol on matrix organization, balancing peptide–polymer interactions.

3.3. In vitro control release and AMP interaction

The release profiles of both CR2109 and resveratrol encapsulated in the ALG/P@Resv/AMP formulation were evaluated under SGF and SIF conditions, as illustrated in Fig. 4 and S3. The data demonstrate the effectiveness of the peptide (CR2109) in enhancing the structural integrity of the encapsulation matrix, thus influencing the release behavior under different pH conditions. In the SIF environment, the ALG/P@Resv/AMP system exhibited an efficient release of resveratrol, reaching almost 100 % within 240 min. The presence of CR2109 acts as a scaffold, stabilizing the nanoparticles that were formed before microencapsulation by spray drying and this structure allows for the controlled diffusion of resveratrol in the neutral pH environment of the intestine, where gradual release is desired (Chen & Zou, 2019). By serving as a structural component, CR2109 not only provides mechanical strength to the matrix but also modulates the release kinetics to ensure that the antioxidant is effectively delivered at the target site. In comparison, the ALG/P@Resv system, which does not contain the peptide scaffold, displayed a slower release rate, reaching approximately 80 % over the same period. This observation highlights the critical role of CR2109 in optimizing the release efficiency and maintaining the integrity of the encapsulation system (Gera et al., 2022).

Under SGF conditions, the formulations exhibited significantly slower release rates. The ALG/P@Resv/AMP system released around 30 % of resveratrol over 240 min, indicating that the peptide scaffold enhances the stability of the encapsulation matrix, particularly in acidic environments. This increased stability prevents premature release in the stomach, ensuring that the resveratrol is protected and retained within the matrix. Such behavior is advantageous as it aligns with the formulation's goal of minimizing release in the gastric setting and focusing release on the intestinal tract (Belščak-Cvitanović et al., 2015). On the other hand, the ALG/P@Resv system, lacking the peptide scaffold, released approximately 40 % of resveratrol, showing that although the alginate-pectin matrix alone provides some degree of protection, the absence of the peptide reduces its ability to withstand the harsh gastric environment as effectively.

The release profile of the antimicrobial peptide CR2109 from the ALG/P@Resv/AMP system further confirms its role as a scaffold. In SIF, the release rate reached approximately 60 % within 120 min, demonstrating that the structure remains intact yet allows controlled release in the neutral environment. This controlled release ensures that the antimicrobial agent is gradually delivered in the intestines, maintaining efficacy over an extended period. In contrast, under SGF conditions, the release of the peptide plateaued at around 20 %, indicating that the structural integrity provided by CR2109 is maintained, thus preventing excessive release and degradation in the stomach.

3.4. Release kinetics analysis

The analysis was performed using several established mathematical models, including Baker-Lonsdale, Higuchi, Korsmeyer-Peppas, and Weibull, each providing insights into the underlying release mechanisms (Table 3). The results reveal distinct release profiles for CR2109 and resveratrol, reflecting their respective roles in antimicrobial action and inflammation control. In the gastric medium, CR2109 exhibited a slower and more controlled release profile compared to resveratrol. The Baker-Lonsdale model provided a poor fit for both compounds, particularly for CR2109 (r^2 = 0.5644), suggesting that spherical diffusion is not the dominant release mechanism in this acidic environment. This is likely due to the strong electrostatic interactions between the positively charged CR2109 and the negatively charged alginate matrix, which form a tighter network that restricts rapid release. Such interactions have been well documented in other peptide-based delivery systems, where ionic interactions between peptides and polysaccharides significantly modulate release kinetics (Herasimenka et al., 2005; Seal & Panitch, 2003).

In contrast, the Higuchi model, which assumes a diffusion-controlled release from a homogenous matrix, showed better agreement with the experimental data for resveratrol (r^2 = 0.5888) than for CR2109 (r^2 = 0.5140). The release constant k was higher for resveratrol (3.8292) compared to CR2109 (3.0699), reflecting a more rapid release of resveratrol in the gastric environment. This is expected, as resveratrol has a smaller molecular size and lower charge, allowing it to diffuse

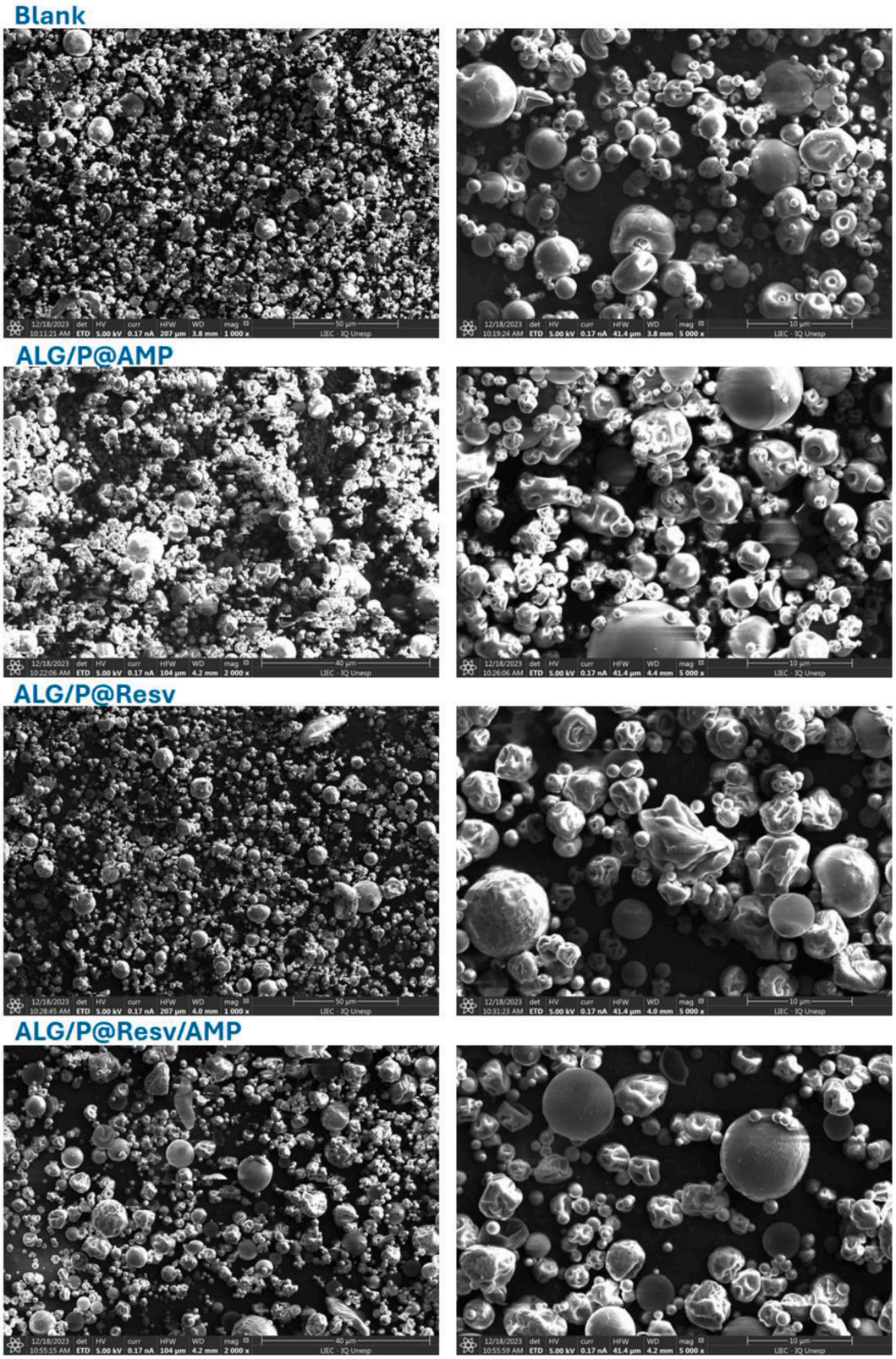

Fig. 3. Scanning Electron Microscopy (SEM) images of the microparticles formulated with alginate and pectin under different conditions: Blank (no actives), ALG/P@Resv, ALG/P@AMP, and ALG/P@Resv/AMP. All images were captured at 5000 × magnification with a scale bar of 10 μm for consistent comparison.

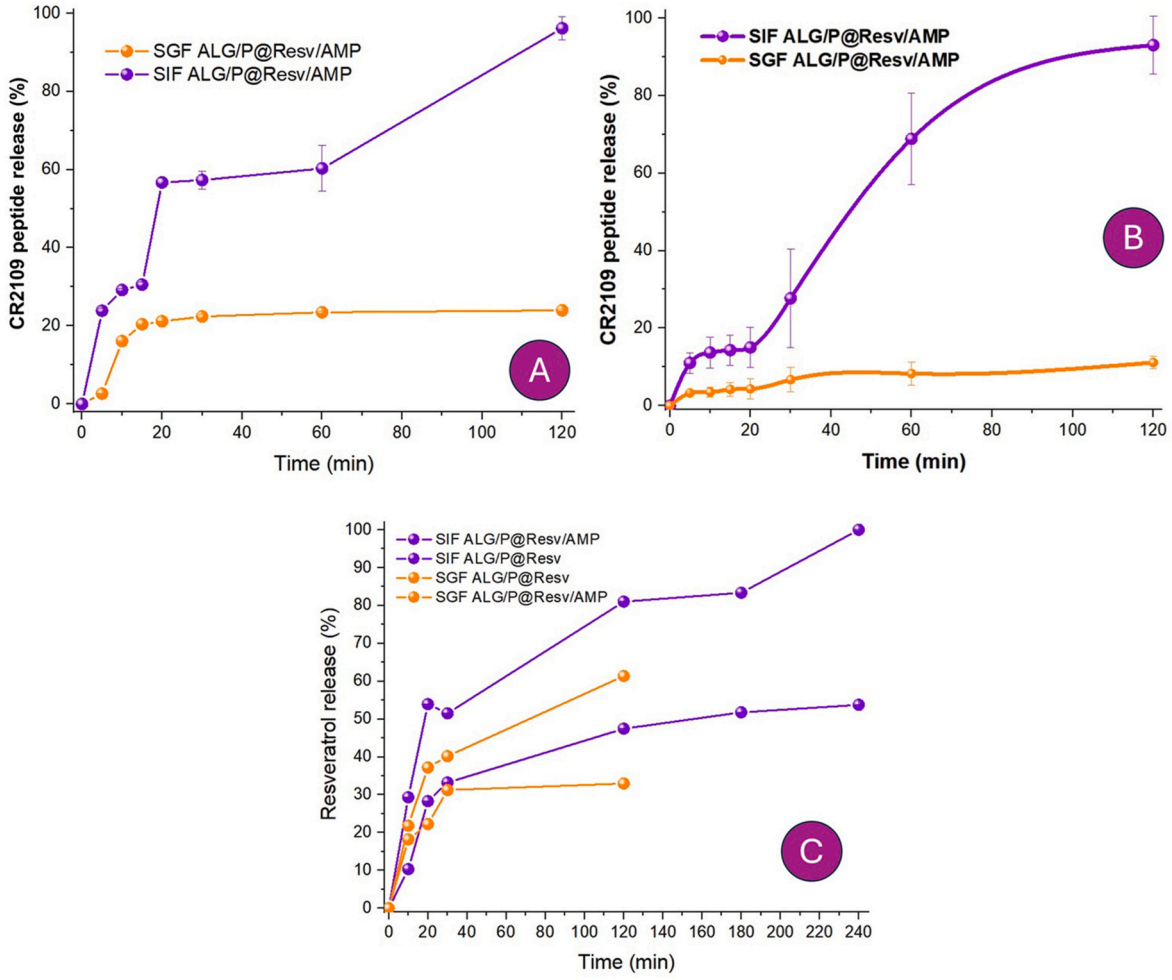

Fig. 4. Controlled release profiles of resveratrol and peptides from microencapsulated formulations in simulated intestinal fluid (SIF) and simulated gastric fluid (SGF). The peptide release profile demonstrates higher release efficiency in SIF compared to SGF, suggesting the formulation's responsiveness to intestinal conditions by **(A)** nanodrop and (B) fluorescamine methods. **(C)** The resveratrol release shows an enhanced release rate in the presence of CR2109 peptide, particularly in SIF, indicating a burst release followed by a plateau.

Table 3
Adjusted correlation coefficient of resveratrol released from microparticles, obtained through different mathematical models for the stages conducted in an acidic (pH 1.2), intestinal (pH 7.4) medium.

Release models	Gastric release system				Intestinal release system		
	ALG/P@Resv/AMP			ALG/P@Resv	ALG/P@Resv		ALG/P@Resv/AMP
	AMP		Resveratrol	Resveratrol	AMP	Resveratrol	Resveratrol
Baker-Lonsdale	k	0.0002	0.0003	0.0009	**0.0022**	0.0004	0.0018
	r^2	0.5644	0.7091	0.9635	**0.9323**	0.9149	0.9601
Higuchi	k	3.0699	3.8292	6.2643	**9.0469**	6.9737	6.9737
	r^2	0.5140	0.5888	0.9155	**0.9237**	0.8591	0.8591
Korsmeyer-Peppas	k	8.3363	**12.8566**	11.9372	**12.2308**	9.1449	10.3133
	r^2	0.7306	**0.9252**	0.9759	**0.9287**	0.9368	0.9419
First-order	n	0.2489	**0.2058**	0.3452	**0.4251**	0.3328	0.5055
	k	0.0039	0.0000	0.0132	0.0275	0.0045	0.0296
	r^2	0.0000	0.0000	0.6781	0.8703	0.5997	0.9099
Hixson- Crowell	k	0.0012	0.0000	0.0034	0.0077	0.0013	0.0061
	r^2	0.0000	0.0000	0.5428	0.8144	0.5374	0.8105
Weibull	k	**23.7335**	33.3956	**180.9000**	139.44	**73.8762**	**53.9258**
	r^2	**0.9975**	0.9202	**0.9980**	0.8507	**0.9997**	**0.9999**
	b	**0.6303**	0.9354	**0.2767**	0.5701	**0.3223**	**0.4746**

Resv: resveratrol. ALG: sodium alginate. P: pectin. AMP: antimicrobial peptide CR2109.

more easily through the alginate matrix. The Korsmeyer-Peppas model provided a better fit for both CR2109 and resveratrol, with r^2 values of 0.7306 and 0.9252, respectively. The release exponent n for CR2109 (0.2489) suggests a predominantly Fickian diffusion mechanism, though the slow release reflects the matrix's ability to hold the peptide in the acidic environment. On the other hand, resveratrol exhibited a more

typical Fickian diffusion profile with $n = 0.2058$, indicating that its release is less influenced by the polymer matrix structure. This is consistent with the behavior of small hydrophobic molecules like resveratrol, which can diffuse more rapidly through polysaccharide-based matrices under acidic conditions (Tian & Liu, 2020). The Weibull model provided the best overall fit for CR2109 in the gastric medium ($r^2 = 0.9975$), with a shape parameter $b = 0.6303$, indicating a bimodal release mechanism involving both diffusion and matrix relaxation. This model's excellent fit reflects the complex nature of peptide release in the presence of alginate, where initial diffusion is slow due to matrix rigidity, followed by a gradual relaxation of the polymer as it begins to swell in the gastric medium.

In the intestinal medium (pH 7.4), both CR2109 and resveratrol exhibited significantly faster release rates. This is expected, as alginate-based systems typically undergo swelling and partial erosion at neutral to basic pH levels, facilitating the release of encapsulated compounds (Volić et al., 2018). The Baker-Lonsdale model showed improved fit for CR2109 ($r^2 = 0.9323$) compared to its performance in the gastric medium. The higher k value (0.0022) for CR2109 in the intestinal environment suggests that the matrix becomes more permeable due to alginate swelling, allowing the peptide to diffuse more freely. This behavior aligns with previous studies where pH-induced alginate swelling has been used to control the release of bioactive compounds in the gastrointestinal tract (Roque-Borda et al., 2023). The Higuchi model demonstrated a strong fit for both CR2109 and resveratrol in the intestinal medium, with r^2 values of 0.9237 and 0.8591, respectively. The higher diffusion constant k for CR2109 (9.0469) indicates a much faster release in this medium, supporting its role in combating pathogenic bacteria in the intestine. The release of resveratrol, though still rapid, remained slightly slower than CR2109, with $k = 6.9737$. This sustained release profile is advantageous for maintaining resveratrol's anti-inflammatory effects over time, as it continues to modulate inflammatory pathways after its initial release (Chen et al., 2020; Davidov-Pardo & McClements, 2014).

The Korsmeyer-Peppas model provided the most useful insights into the release mechanisms in the intestinal medium. For CR2109, the release exponent $n = 0.4251$ suggests anomalous diffusion, where both diffusion and matrix relaxation govern the release. This controlled release profile ensures that CR2109 remains active over a prolonged period in the intestine, providing continuous antimicrobial action, which is essential for combating pathogenic bacteria that cause inflammation in the gut. resveratrol's release also followed an anomalous diffusion pattern, with $n = 0.5055$, indicating a balance between rapid initial release and sustained activity. This release profile is particularly important for inflammatory conditions like inflammatory bowel disease (IBD), where both rapid and prolonged anti-inflammatory actions are required (Lopes et al., 2023). The Weibull model, once again, provided an excellent fit for both CR2109 and resveratrol in the intestinal medium. The shape parameter $b = 0.5701$ for CR2109 and $b = 0.4746$ for resveratrol indicates a complex release mechanism, likely involving initial diffusion followed by matrix erosion. This is consistent with the behavior of alginate-based microparticles, which swell and partially degrade in the intestinal environment, leading to a sustained release over time (Hosseini et al., 2014).

The results reflect the critical role of the spray drying process in shaping the release profiles of CR2109 and resveratrol. The dehydration that occurs during spray drying leads to the formation of a compact outer shell, which controls the initial burst release, particularly for smaller compounds like resveratrol. The nanoassembly behavior of CR2109 with alginate and pectin results in a dense matrix, which slows down the release of the peptide, particularly in the gastric medium. However, in the intestinal medium, the partial erosion of the alginate matrix allows the release of both compounds in a controlled, sustained manner (Gartziandia et al., 2018). These findings align with previous studies that have shown the importance of self-assembly and spray drying in achieving multi-phase release behavior in biopolymer-based delivery systems (Marante et al., 2020). It was previously demonstrated that systems that incorporate pectin significantly improve mucoadhesion and maintain a better release of the encapsulated compounds, and this is how the results of this article are reflected (Bagliotti Meneguin et al., 2014; Meneguin et al., 2024). The results from the mathematical models provide a clear understanding of how CR2109 and resveratrol behave within the formulated microparticles containing self-assembled peptides in both gastric and intestinal media. The controlled release of CR2109 in the intestinal medium positions it as a strong candidate for combating pathogenic bacteria, while the rapid and sustained release of resveratrol ensures that it can effectively manage inflammation.

3.5. Antimicrobial efficacy of CR2109 against bacterial strains

MIC values of the CR2109 peptide against various strains of *E. coli, Klebsiella* sp., and *Salmonella* sp. are summarized in Table 4. The MIC values highlight the peptide's differential efficacy against strains with varying resistance profiles, including multidrug-resistant (MDR) strains. CR2109 demonstrated potent antimicrobial activity against the quality control strain *E. coli* ATCC 25922, with a MIC value of 11.04 μg/mL. This result is consistent with expected susceptibility levels in non-resistant, standardized strains. The low MIC value indicates the peptide's effectiveness at low concentrations when no resistance mechanisms are present. CR2109 showed effective activity against the MDR strain *S.* Typhimurium F98, with a MIC of 5.44 μg/mL. This strain, known for its multidrug resistance, still exhibited a significant level of susceptibility to CR2109, suggesting that despite its MDR profile, the mechanisms employed by the F98 strain do not completely inhibit the peptide's action. This result indicates that CR2109 may bypass certain resistance pathways present in this strain, maintaining its antimicrobial potency.

For other MDR strains, including *E. coli* $bla_{\text{CTX-M-2}}$, *S.* Mbandaka, *K. pneumoniae* ($bla_{\text{NDM-1}}$), and *K. pneumoniae* MDR, MIC values were notably higher (100 μg/mL or >100 μg/mL). These strains possess various antimicrobial resistance genes, such as beta-lactamases (e.g., $bla_{\text{CTX-M-2}}$, $bla_{\text{NDM-1}}$) and colistin resistance genes (e.g., *mcr-1*), which likely impact the peptide's ability to interact with the bacterial membrane or evade enzymatic degradation. The variation in MIC values demonstrates that while CR2109 is effective against some MDR strains like *S.* Typhimurium F98, its activity is significantly reduced against other MDR strains. This underscores the need to understand and target specific resistance mechanisms that limit the peptide's efficacy. Modifying CR2109 to increase its membrane penetration ability, protect it from enzymatic degradation, or employ combination therapies could enhance its performance against more resistant bacterial strains (Abraham et al., 2014). The MIC results show that CR2109 retains activity against certain MDR strains, such as *S.* Typhimurium F98, but is less effective against others, particularly those harboring resistance genes like $bla_{\text{CTX-M-2}}$, $bla_{\text{NDM-1}}$, and *mcr-1*. To increase its therapeutic potential, future studies should focus on structural modifications and combination treatments aimed at overcoming these resistance barriers.

Table 4
Minimal inhibitory concentrations of CR2109 against *E. coli, Klebsiella* sp. and *Salmonella* sp. strains at concentrations in the range 2–250 μg/mL.

Bacteria strain	MIC value (μg/mL)
E. coli ATCC 25922	11.04
S. Typhimurium F98	5.44
E. coli $bla_{\text{CTX-M-2}}$	100
S. Mbandaka MDR	100
S. Minnesota MDR	>100
E. coli mcr-1	>100
E. coli C600	>100
K. pneumunie NDM+	>100
K. pneumunie MDR	>100

3.6. Antioxidant activity and cytotoxicity evaluation

The antioxidant activity of the formulations and their components reveals significant variability, highlighting the influence of the microencapsulation process and the presence of bioactive agents like resveratrol and the antimicrobial peptide CR2109. ALG/P@Resv and pure resveratrol showed high antioxidant activities, with values of 78.45 ± 0.82 % and 86.44 ± 0.14 %, respectively (Table 5). This similarity indicates that the encapsulation process preserves the bioactivity of resveratrol effectively (Zhong et al., 2022). The minor reduction in activity in the ALG/P@Resv formulation compared to pure resveratrol might be due to interactions between the alginate-pectin matrix and the compound, which could slightly limit its free radical scavenging efficiency (Mendes et al., 2012).

In contrast, the formulations ALG/P@AMP and CR2109 showed low antioxidant activities, with values close to the blank control (approximately 11–12 %). This confirms that CR2109, primarily an antimicrobial peptide, does not possess significant antioxidant properties. The low activity of ALG/P@AMP suggests that the encapsulation of CR2109 alone does not enhance the formulation's antioxidant potential, consistent with its mechanism of action focused on antimicrobial efficacy rather than radical scavenging. The combined formulation, ALG/P@Resv/AMP, displayed the highest antioxidant activity (88.74 ± 0.33 %), surpassing both ALG/P@Resv and pure resveratrol. This increase implies a synergistic effect between the peptide and resveratrol when encapsulated together, possibly enhancing the stability and controlled release of the antioxidant (Liu et al., 2020). This synergistic behavior aligns with previous findings where multi-functional encapsulation systems improved the bioactivity of combined components (Derakhshan-sefidi et al., 2024). On the other hand, both ALG/P@Resv and ALG/P@Resv/AMP formulations exhibited minimal cytotoxicity, maintaining cell viability above 90 % at the tested concentration of 500 μg/mL and the high viability observed suggests that the presence of resveratrol, even when combined with CR2109, does not adversely affect macrophages.

During inflammation, reactive oxygen species (ROS) are generated as a response of the organism to eliminate pathogens, however, an uncontrolled process can damage tissues and cells, worsening the situation of the host (Chelombitko, 2018). In this sense, antioxidants play an important role during inflammation caused by pathogens, neutralizing these ROS. Although there is an interrelation between antioxidants and anti-inflammatories, not all compounds with one of these properties necessarily have the other and the specificity of each molecule and its mechanism of action determines whether it can fulfill both functions or only one of them (Fuller, 2022). Previous studies highlight the use of resveratrol to counteract inflammation, which allows us to affirm its use during a process-induced *in vivo* models (Baur & Sinclair, 2006; Chen et al., 2019). On the other hand, CR2109 barely shows antibacterial activity in micrometric concentrations, which in turn would be useful to implement a multifunctional system in the control of intestinal pathogens. In an *in vitro* complete analysis of the results shown so far, the peptide would be acting as a scaffold that is part of this microencapsulated reinforcement which would allow a better release without harmful effects for an effective treatment (Karamat-Ullah et al., 2021; Zhang et al., 2018).

In summary, the peptide was synthesized and exhibits antimicrobial activity even against resistant strains. It also shows antioxidant activity, which is linked to its anti-inflammatory effects. The analysis of the nano-assembled system, incorporating the peptide and loaded with resveratrol within a matrix of alginate and pectin microparticles, demonstrates its ability to control and protect the resveratrol, while the peptide self-protects against various factors that could lead to the instability or degradation of both bioactive compounds. Additionally, this system is non-cytotoxic to macrophages, which could allow for a more effective treatment against intracellular bacteria.

Table 5
Antioxidant activity (after 2h) and cytotoxicity (after 12h) were calculated in the range of 31.25–500 μg/mL of each sample.

Sample	Antioxidant activity (I%)	Half maximal inhibitory concentration (IC50, μg/mL)
Blank	10.48 ± 0.04	>500
ALG/P@Resv	78.45 ± 0.82	>500
ALG/P@AMP	11.29 ± 0.85	>500
ALG/P@Resv/AMP	88.74 ± 0.33	>500
CR2109	11.20 ± 0.02	>500
Resveratrol	86.44 ± 0.14	>500

3.7. Efficacy of self-assembly microencapsulated compounds in Galleria mellonella model

The use of *G. mellonella* as an infection model provides valuable insights into the efficacy and biocompatibility of the microencapsulated compounds (ALG/P@Resv, ALG/P@AMP, and ALG/P@Resv/AMP) against *S.* Typhimurium (Gourkhede et al., 2022). The survival assays and histological evaluations collectively demonstrate the potential of these formulations as effective therapeutic agents, capable of modulating inflammatory responses and providing antimicrobial protection. The survival curves presented in Fig. 5 (A, B, and C) reveal important patterns regarding the toxicity and therapeutic potential of the formulated microparticles containing self-assembled peptides.

The survival rates of larvae exposed to microencapsulated compounds at 500 μg/mL indicate no adverse effects across all tested formulations (ALG/P, ALG/P@AMP, ALG/P@Resv, and ALG/P@Resv/AMP). The survival rates were consistent with those of the negative control (PBS), suggesting that the encapsulation process and the active compounds (resveratrol and CR2109) are well-tolerated by the larvae and this finding supports the biocompatibility of the microencapsulated systems, highlighting their potential for therapeutic applications without inducing cytotoxicity (Spósito et al., 2024). The survival rates of larvae infected with *S.* Typhimurium at varying CFU levels (10^2, 10^3, and 10^4 CFUs) illustrate a clear dose-response relationship. At lower CFU counts (10^2), the larvae maintained a moderate survival rate, indicating a manageable immune response. However, at higher bacterial loads (10^3 and 10^4 CFUs), the survival rate drastically decreased within 1–2 days, demonstrating the virulence of the pathogen and its capacity to overwhelm the larvae's immune defenses. This data underscores the relevance of the *G. mellonella* model for studying pathogenicity and evaluating the efficacy of antimicrobial agents in a controlled infection environment.

The therapeutic potential of the formulations was further evaluated in larvae infected with 10^2 CFUs of *S.* Typhimurium. The survival rates following treatment with a single dose of the formulations indicate that the combined formulation ALG/P@Resv/AMP had the highest protective effect, closely matching that of the positive control. This suggests a synergistic action between resveratrol and the CR2109 peptide, providing effective antimicrobial and anti-inflammatory effects. The individual formulations (ALG/P@AMP and ALG/P@Resv) offered moderate protection, indicating that while each component contributes to the therapeutic outcome, their combination maximizes efficacy. These results align with existing literature that highlights the enhanced effects of combining antimicrobial peptides with antioxidants, demonstrating the potential of such formulations to achieve better therapeutic outcomes (Choi et al., 2024).

Histological examination of *G. mellonella* larvae post-LPS induction and treatment with the microencapsulated formulations (Fig. 5D and E) provides further evidence of the anti-inflammatory and therapeutic effects. The top histological image shows LPS-induced inflammation characterized by dense infiltration of hemocytes and immune cells, particularly in the cuticular and muscle regions. Notably, granulomas—aggregates of immune cells that form in response to persistent

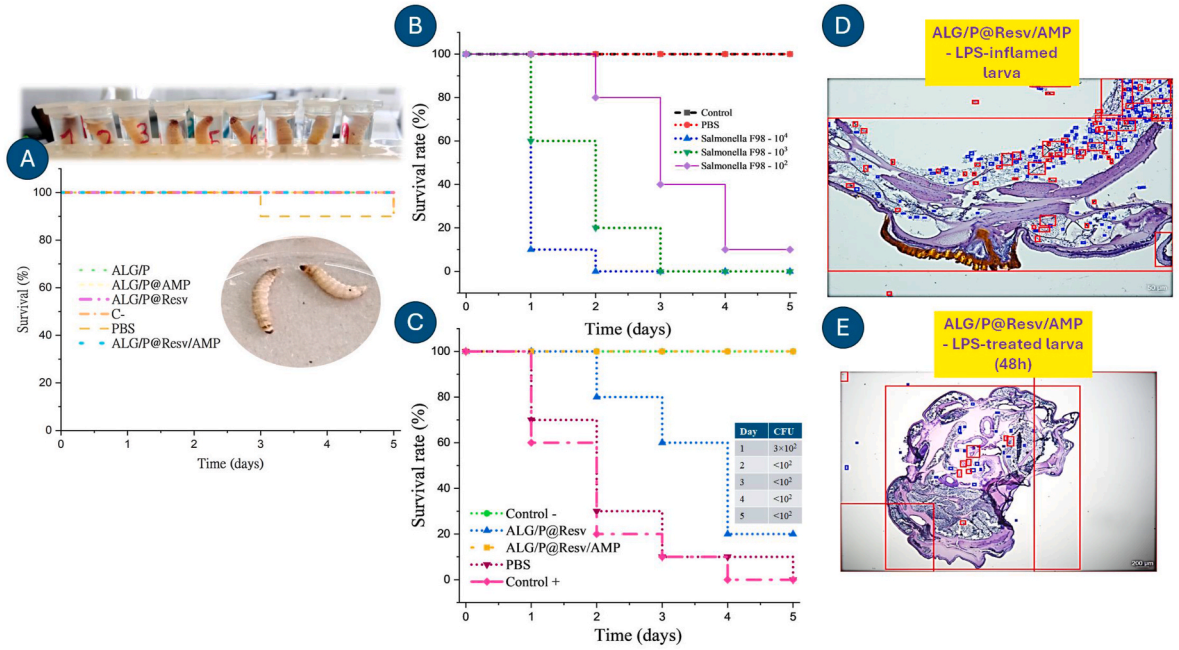

Fig. 5. (A) Survival curve based on the microencapsulated compounds evaluated at 500 μg/mL and **(B)** the survival rate against bacterial infection with *S.* Typhimurium at different colony-forming unit concentrations. **(C)** Survival after infection and treatment for 5 days at a single dose. Each result shown was performed in separate experiments. **(D)** Histology of larvae during infection and **(E)** after treatment with samples.

inflammation—are visible, indicating an active inflammatory response (Herbath et al., 2021). However, following treatment with the ALG/-P@Resv/AMP formulation, the number and size of granulomas are significantly reduced, suggesting that the formulation is effective in modulating the inflammatory response. This reduction in granuloma formation highlights the anti-inflammatory potential of the formulation, likely due to the antioxidant effects of resveratrol and the immune-modulatory properties of CR2109, which work together to control and diminish the inflammation process.

The histological cross-section observed at 48 h post-treatment with ALG/P@Resv/AMP reveals a substantial decrease in inflammatory cell presence and a notable reduction in granulomas compared to earlier time points. The tissue architecture is preserved, with reduced immune cell infiltration and inflammation, indicating effective resolution of the inflammatory response. This suggests that the controlled release of resveratrol and CR2109 within the encapsulated formulation maintains therapeutic levels over time, facilitating tissue recovery and minimizing chronic inflammation. The observed anti-inflammatory and protective effects reinforce the potential of this formulation for treating infections and associated inflammatory conditions (Asai et al., 2023). The combined data from the survival assays and histological analysis demonstrate the efficacy of the ALG/P@Resv/AMP formulation in providing both antimicrobial and anti-inflammatory benefits. The effect between the antioxidant properties of resveratrol and the antimicrobial peptide CR2109 enhances therapeutic outcomes, supporting the hypothesis that multi-functional microparticles can be effective in managing both infection and inflammation. The ability of this formulation to reduce granulomas and promote tissue recovery further underscores its potential for clinical applications, particularly in gastrointestinal settings where inflammation control and bacterial eradication are crucial. Future studies should focus on optimizing these formulations for *in vivo* applications, maximizing their stability and therapeutic efficacy.

The comprehensive evaluation of *G. mellonella* as an infection and inflammation model highlights the therapeutic potential of microencapsulated formulations like ALG/P@Resv/AMP. The combined antimicrobial and anti-inflammatory actions observed, including the reduction of granulomas, support the continued development of such formulations for treating infections accompanied by inflammatory responses (Pereira et al., 2020).

4. Conclusions

The study comprehensively evaluates the antimicrobial and anti-inflammatory potential of microencapsulated formulations containing resveratrol and the antimicrobial peptide CR2109, using the *G. mellonella* infection model. The results indicate that these formulations are well-tolerated, exhibiting no cytotoxic effects at the tested concentrations, and effectively enhancing the survival of larvae infected with *S.* Typhimurium. Notably, the combined formulation ALG/P@Resv/AMP demonstrated the most potent therapeutic effect, significantly improving survival rates and reducing inflammation markers, including granuloma formation. The histological analysis further confirms that this formulation modulates the inflammatory response, promoting tissue recovery and maintaining structural integrity over time. These findings highlight the effect between the antioxidant properties of resveratrol and the antimicrobial activity of CR2109, underscoring the advantages of multi-functional encapsulated systems for managing both infection and inflammation. The study supports the potential of such formulations for clinical applications, particularly for gastrointestinal infections where controlled release and dual-action (antimicrobial and anti-inflammatory) properties are beneficial. Future research should focus on optimizing the encapsulation process and dosage to maximize therapeutic outcomes, paving the way for developing effective treatments against multidrug-resistant pathogens and associated inflammatory conditions.

CRediT authorship contribution statement

Cesar Augusto Roque-Borda: Writing – original draft, Validation, Methodology, Investigation, Funding acquisition, Formal analysis, Data curation, Conceptualization. **Marco Roberto Chávez-Morán:** Methodology, Investigation. **Laura Maria Duran Gleriani Primo:** Methodology, Investigation. **José C.E. Márquez Montesinos:** Methodology, Investigation. **Vinicius Martinho Borges Cardoso:** Methodology,

Investigation. **Mauro M.S. Saraiva:** Methodology, Investigation. **Caroline Maria Marcos:** Methodology, Investigation. **Marlus Chorilli:** Methodology, Investigation. **Fernando Albericio:** Visualization, Validation, Supervision. **Beatriz G. de la Torre:** Writing – review & editing, Visualization, Validation, Supervision. **Fernando Rogério Pavan:** Writing – review & editing, Visualization, Validation, Supervision, Resources, Project administration, Investigation. **Andréia Bagliotti Meneguin:** Methodology, Investigation.

Declaration of competing interest

All contributing authors declare no conflicts of interest.

Acknowledgments

This study was supported by the São Paulo Research Foundation (FAPESP): Research Grant: 2023/01664-1 and Fellowships: 2020/16573-3, 2021/14603-5. This study was financed in part by the Coordenação de Aperfeiçoamento de Pessoal de Nível Superior – Brasil (CAPES). The authors also thank the "I International Internship Contest 2023-II" which promotes the exchange of students in laboratories abroad, a grant awarded by the "Universidad Nacional de Frontera". The authors also thank ChatGPT 4 - DALL-E tool that was used to develop the Graphical Abstract and to correct the English grammar.

Appendix A. Supplementary data

Supplementary data to this article can be found online at https://doi.org/10.1016/j.foodhyd.2025.111454.

Data availability

Data will be made available on request.

References

Abraham, P., George, S., & Kumar, K. S. (2014). *Biochimie, 97*, 144.
Adasme, M. F., Linnemann, K. L., Bolz, S. N., Kaiser, F., Salentin, S., Haupt, V. J., & Schroeder, M. (2021). *Nucleic Acids Research, 49*, Article W530.
Al Musaimi, O., de la Torre, B. G., & Albericio, F. (2020). *Green Chemistry, 22*, 996.
Allué-Guardia, A., Nyong, E. C., Koenig, S. S. K., Vargas, S. M., Bono, J. L., & Eppinger, M. (2019). *Microbiology Resource Announcements, 8*.
Anbinder, P. S., Deladino, L., Navarro, A. S., Amalvy, J. I., & Martino, M. N. (2011). *Journal of Encapsulation and Adsorption Sciences, 1*, 80.
Aronica, P. G. A., Reid, L. M., Desai, N., Li, J., Fox, S. J., Yadahalli, S., Essex, J. W., & Verma, C. S. (2021). *Journal of Chemical Information and Modeling, 61*, 3172.
Asai, M., Li, Y., Newton, S. M., Robertson, B. D., & Langford, P. R. (2023). *FEMS Microbiology Reviews, 47*.
Bagliotti Meneguin, A., Stringhetti Ferreira Cury, B., & Evangelista, R. C. (2014). *Carbohydrate Polymers, 99*, 140.
Barajas-Álvarez, P., González-Ávila, M., & Espinosa-Andrews, H. (2023). *Food Reviews International, 39*, 992.
Barrow, P. A., Hassan, J. O., & Berchieri, A. (1990). *Epidemiology and Infection, 104*, 413.
Baur, J. A., & Sinclair, D. A. (2006). *Nature Reviews Drug Discovery, 5*, 493.
Bazán, J. M. N., Chagas, V. L., Silva, R. G., Silva, I. S. S., Araujo, J. G. N., … dos Santos Silva, L. (2023). Development and characterization of alginate-derived bioadhesive films incorporated with anti-infective lectins for application in the treatment of oral candidiasis. *Journal of Drug Delivery Science and Technology, 90*, 105114.
Bélanger, D., Tong, X., Soumaré, S., Dory, Y. L., & Zhao, Y. (2009). *Chemistry - A European Journal, 15*, 4428.
Belščak-Cvitanović, A., Đorđević, V., Karlović, S., Pavlović, V., Komes, D., Ježek, D., Bugarski, B., & Nedović, V. (2015). *Food Hydrocolloids, 51*, 361.
Benevides, V. P., Saraiva, M. M. S., Nascimento, C. F., Delgado-Suárez, E. J., Oliveira, C. J. B., Silva, S. R., Miranda, V. F. O., Christensen, H., Olsen, J. E., & Berchieri Junior, A. (2024). *Microorganisms, 12*, 312.
Bergonzi, C., d'Ayala, G. G., Elviri, L., Laurienzo, P., Bandiera, A., & Catanzano, O. (2020). *International Journal of Biological Macromolecules, 164*, 586.
Berman, H. M. (2000). *Nucleic Acids Research, 28*, 235.
Bodbodak, S., Nejatian, M., Ghandehari Yazdi, A. P., Kamali Rousta, L., Rafiee, Z., Jalali-Jivan, M., Kharazmi, M. S., & Jafari, S. M. (2024). *Critical Reviews in Food Science and Nutrition, 64*, 2824.
Chelombitko, M. A. (2018). *Moscow University Biological Sciences Bulletin, 73*, 199.
Chen, S., Han, Y., Jian, L., Liao, W., Zhang, Y., & Gao, Y. (2020). *Carbohydrate Polymers, 236*, Article 116090.
Chen, F., Liu, H., Sun, H., Pan, P., Li, Y., Li, D., & Hou, T. (2016). *Physical Chemistry Chemical Physics, 18*, Article 22129.
Chen, C.-H., Wang, F.-Y., Mao, C.-F., Liao, W.-T., & Hsieh, C.-D. (2008). *International Journal of Biological Macromolecules, 43*, 37.
Chen, L., Xu, W., Yang, Z., McClements, D. J., Peng, X., Xu, Z., Meng, M., Zou, Y., Chen, G., & Jin, Z. (2024). *International Journal of Biological Macromolecules, 278*, Article 134827.
Chen, L. Z., Yao, L., Jiao, M. M., Shi, J. B., Tan, Y., Ruan, B. F., & Liu, X. H. (2019). *European Journal of Medicinal Chemistry, 175*, 114.
Chen, K., & Zhang, H. (2019). *International Journal of Biological Macromolecules, 136*, 936.
Chen, J., & Zou, X. (2019). *Bioactive Materials, 4*, 120.
Choi, S., Han, S., Lee, S., Kim, J., Kim, J., & Kang, D.-K. (2024). *Antioxidants, 13*, 447.
Chung, C.-R., Kuo, T.-R., Wu, L.-C., Lee, T.-Y., & Horng, J.-T. (2020). *Briefings in Bioinformatics, 21*, 1098.
C. L. S. I. P. (2018). In *, 1. Standards for Antimicrobial Susceptibility Testing CLSI, M100 Performance Standards for Antimicrobial Susceptibility Testing*.
Costa, H. D. S., & Dias, M. R. (2021). Alginate/bioactive glass beads: synthesis, morphological and compositional changes caused by SBF immersion method. *Materials Research, 24*(4), Article e20200587.
da Costa de Souza, G., Roque-Borda, C. A., & Pavan, F. R. (2022). Beta-lactam resistance and the effectiveness of antimicrobial peptides against KPC-producing bacteria. *Drug Development Research, 83*(7), 1534–1554.
Davidov-Pardo, G., & McClements, D. J. (2014). *Trends in Food Science & Technology, 38*, 88.
Deladino, L., Anbinder, P. S., Navarro, A. S., & Martino, M. N. (2008). *Carbohydrate Polymers, 71*, 126.
Deng, H., Zhang, S., Fu, Y., Dong, N., Bi, C., Shan, A., & Shao, C. (2024). *Chemical Engineering Journal, 496*, Article 154232.
Derakhshan-sefidi, M., Bakhshi, B., & Rasekhi, A. (2024). *BMC Microbiology, 24*, 257.
Ding, M.-H., Xu, P.-G., Wang, Y., Ren, B., & Zhang, J.-L. (2023). *Immunological Investigations, 52*, 194.
Emery, H., Johnston, R., Rowley, A. F., & Coates, C. J. (2019). *Archives of Toxicology, 93*, 2347.
Fan, Y., Yu, Z., Zhao, W., Ding, L., Zheng, F., Li, J., & Liu, J. (2020). *Food Science and Human Wellness, 9*, 257.
Fichman, G., & Gazit, E. (2014). *Self-assembly of short peptides to form hydrogels: Design of building blocks, physical properties and technological applications* (Vol. 10). Elsevier BV.
Flamminii, F., Paciulli, M., Di Michele, A., Littardi, P., Carini, E., Chiavaro, E., Pittia, P., & Di Mattia, C. D. (2021). *Current Research in Food Science, 4*, 698.
Fuller, B. B. (2022). In *Cosmetic dermatology* (pp. 366–387). Wiley.
Galán, J. E. (2021). *Nature Reviews Microbiology, 19*, 716.
Gartziandia, O., Lasa, A., Pedraz, J. L., Miranda, J., Portillo, M. P., Igartua, M., & Hernández, R. M. (2018). *Molecules, 23*, 1886.
Gasteiger, E., Hoogland, C., Gattiker, A., Duvaud, S., Wilkins, M. R., Appel, R. D., & Bairoch, A. (2005). In *The proteomics protocols handbook* (pp. 571–607). Totowa, NJ: Springer.
A. Gautam, K. Chaudhary, R. Kumar, G. P. S. Raghava, 2015, pp. 59–69.
Gautam, A., Chaudhary, K., Kumar, R., Sharma, A., Kapoor, P., Tyagi, A., & Raghava, G. P. S. (2013). *Journal of Translational Medicine, 11*, 74.
Gawde, U., Chakraborty, S., Waghu, F. H., Barai, R. S., Khanderkar, A., Indraguru, R., Shirsat, T., & Idicula-Thomas, S. (2023). *Nucleic Acids Research, 51*, Article D377.
Gera, S., Kankuri, E., & Kogermann, K. (2022). *Pharmacology & Therapeutics, 232*, Article 107990.
Gourkhede, D. P., Dani Nishanth, M. A., Ram, V. P., Abishad, P., Yasur, J., Pollumahanti, N., Vergis, J., Singh Malik, S. V., Barbuddhe, S. B., & Rawool, D. B. (2022). *Journal of Drug Delivery Science and Technology, 78*, Article 103981.
Gowd, V., Kanika, Jori, C., Chaudhary, A. A., Rudayni, H. A., Rashid, S., & Khan, R. (2022). *The Journal of Nutritional Biochemistry, 109*, Article 109101.
Haneishi, Y., Furuya, Y., Hasegawa, M., Picarelli, A., Rossi, M., & Miyamoto, J. (2023). *International Journal of Molecular Sciences, 24*, 3817.
Herasimenka, Y., Benincasa, M., Mattiuzzo, M., Cescutti, P., Gennaro, R., & Rizzo, R. (2005). *Peptides (N.Y.), 26*, 1127.
Herbath, M., Fabry, Z., & Sandor, M. (2021). *Biology Futur, 72*, 61.
Higashiyama, M., & Hokaria, R. (2023). *Digestion, 104*, 74.
Hole, B. B., Schwarz, J. A., Gilbert, J. L., & Atkinson, B. L. (2005). *Journal of Biomedical Materials Research Part A, 74A*, 712.
Honorato, R. V., Koukos, P. I., Jiménez-García, B., Tsaregorodtsev, A., Verlato, M., Giachetti, A., Rosato, A., & Bonvin, A. M. J. J. (2021). *Frontiers in Molecular Biosciences, 8*.
Honorato, R. V., Trellet, M. E., Jiménez-García, B., Schaarschmidt, J. J., Giulini, M., Reys, V., … Bonvin, A. M. (2024). The HADDOCK2. 4 web server for integrative modeling of biomolecular complexes. *Nature protocols, 19*(11), 3219–3241.
Hosseini, S. M., Hosseini, H., Mohammadifar, M. A., German, J. B., Mortazavian, A. M., Mohammadi, A., Khosravi-Darani, K., Shojaee-Aliabadi, S., & Khaksar, R. (2014). *Carbohydrate Polymers, 103*, 573.
Hou, T., Wang, J., Li, Y., & Wang, W. (2011). *Journal of Chemical Information and Modeling, 51*, 69.
Huang, X., Dai, Y., Cai, J., Zhong, N., Xiao, H., McClements, D. J., & Hu, K. (2017). *Food Hydrocolloids, 64*, 157.
Iqbal, Y., Amin, F., Aziz, M. H., & Wahab, R. (2024). *International Journal of Biological Macromolecules, 280*, Article 135656.
Jeong, H., Samdani, K. J., Yoo, D. H., Lee, D. W., Kim, N. H., Yoo, I.-S., & Lee, J. H. (2016). *International Journal of Biological Macromolecules, 93*, 757.
Jiménez-García, B., Roel-Touris, J., Romero-Durana, M., Vidal, M., Jiménez-González, D., & Fernández-Recio, J. (2018). *Bioinformatics, 34*, 49.

Karamat-Ullah, N., Demidov, Y., Schramm, M., Grumme, D., Auer, J., Bohr, C., Brachvogel, B., & Maleki, H. (2021). *ACS Biomaterials Science & Engineering, 7*, 4545.
Khor, B., Gardet, A., & Xavier, R. J. (2011). *Nature, 474*, 307.
Krishnanand, K. N., & Ghose, D. (2009). *Swarm Intelligence, 3*, 87.
Lang, P. T., Brozell, S. R., Mukherjee, S., Pettersen, E. F., Meng, E. C., Thomas, V., Rizzo, R. C., Case, D. A., James, T. L., & Kuntz, I. D. (2009). *RNA, 15*, 1219.
Lengyel, M., Kállai-Szabó, N., Antal, V., Laki, A. J., & Antal, I. (2019). *Scientia Pharmaceutica, 87*, 20.
Levin, A., Hakala, T. A., Schnaider, L., Bernardes, G. J. L., Gazit, E., & Knowles, T. P. J. (2020). *Nature Reviews Chemistry, 4*, 615.
Lin, T.-T., Yang, L.-Y., Lu, I.-H., Cheng, W.-C., Hsu, Z.-R., Chen, S.-H., & Lin, C.-Y. (2021). *mSystems, 6*.
Liu, Y., Liang, X., Zou, Y., Peng, Y., McClements, D. J., & Hu, K. (2020). *Food & Function, 11*, 4014.
Liu, S., Zhang, C., Zhou, H., & Zhou, Y. (2004). *Proteins: Structure, Function, and Bioinformatics, 56*, 93.
Lopes, S. A., Cardoso, V. M. B., Roque-Borda, C. A., Chorilli, M., & Meneguin, A. B. (2025). *International Journal of Biological Macromolecules, 291*, Article 139060.
Lopes, S. A., Roque-Borda, C. A., Duarte, J. L., Di Filippo, L. D., Borges Cardoso, V. M., Pavan, F. R., Chorilli, M., & Meneguin, A. B. (2023). *Pharmaceutics, 15*, 2600.
Mancer, D., & Daoud, K. (2021). *Pharmaceutical Chemistry Journal, 55*, 954.
Manjili, Z. N., Mahoonak, A. S., Ghorbani, M., Tabarestani, H. S., & Moghadam, V. E. (2024). *Current Research in Food Science, 8*, Article 100739.
Marangoni Júnior, L., Fozzatti, C. R., Jamróz, E., Vieira, R. P., & Alves, R. M. V. (2022). *Materials, 15*, 3881.
Marante, T., Viegas, C., Duarte, I., Macedo, A. S., & Fonte, P. (2020). *Pharmaceutics, 12*, 1032.
Mendes, J. B. E., Riekes, M. K., De Oliveira, V. M., Michel, M. D., Stulzer, H. K., Khalil, N. M., Zawadzki, S. F., Mainardes, R. M., & Farago, P. V. (2012). *The Scientific World Journal*, 2012.
Meneguin, A. B., Roque-Borda, C. A., Piperas, A. B. G., Pollini, M. F. O., Cardoso, V. M. B., Primo, L. M. D. G., Alemi, F., Pavan, F. R., & Chorilli, M. (2024). *Carbohydrate Polymers, 346*, Article 122647.
Mirtič, J., Ilaš, J., & Kristl, J. (2018). *Carbohydrate Polymers, 181*, 93.
Mooney, C., Haslam, N. J., Pollastri, G., & Shields, D. C. (2012). *PLoS One, 7*, Article e45012.
Moreira Lopes, T. C., Mosser, D. M., & Gonçalves, R. (2020). *Inflammation Research, 69*, 1163.
Morena, F., Cencini, C., Calzoni, E., Martino, S., & Emiliani, C. (2024). *Biomolecules, 14*, 930.
Mormile, C., Opriș, O., Bellucci, S., Lung, I., Kacso, I., Turza, A., Stegarescu, A., Tripon, S., Soran, M.-L., & Bâldea, I. (2024). *Gels, 11*, 15.
Moustakas, D. T., Lang, P. T., Pegg, S., Pettersen, E., Kuntz, I. D., Brooijmans, N., & Rizzo, R. C. (2006). *Journal of Computer-Aided Molecular Design, 20*, 601.
Ochbaum, G., & Bitton, R. (2017). *Polymer (Guildf), 108*, 87.
Pan, J., Li, Y., Chen, K., Zhang, Y., & Zhang, H. (2021). *Carbohydrate Polymers, 266*, Article 118102.
Pereira, M. F., Rossi, C. C., da Silva, G. C., Rosa, J. N., & Bazzolli, D. M. S. (2020). *Pathogens Disease, 78*.
Pettersen, E. F., Goddard, T. D., Huang, C. C., Couch, G. S., Greenblatt, D. M., Meng, E. C., & Ferrin, T. E. (2004). *Journal of Computational Chemistry, 25*, 1605.
Polinário, G., Primo, L. M. D. G., Rosa, M. A. B. C., Dett, F. H. M., Barbugli, P. A., Roque-Borda, C. A., & Pavan, F. R. (2023). *Frontiers in Microbiology, 14*.
Primo, L. M. D. G., Roque-Borda, C. A., Carnero Canales, C. S., Caruso, I. P., de Lourenço, I. O., Colturato, V. M. M., Sábio, R. M., de Melo, F. A., Vicente, E. F., Chorilli, M., da Silva Barud, H., Barbugli, P. A., Franzyk, H., Hansen, P. R., & Pavan, F. R. (2024). *Carbohydrate Polymers, 323*, Article 121449.
Qi, G., Gao, Y., Wang, L., & Wang, H. (2018). *Advanced Materials, 30*.
Raheem, A., Liang, L., Zhang, G., & Cui, S. (2021). *Frontiers in Immunology, 12*.
Rathore, A. S., Choudhury, S., Arora, A., Tijare, P., & Raghava, G. P. S. (2024). *Computers in Biology and Medicine, 179*, Article 108926.
Rey, J., Murail, S., de Vries, S., Derreumaux, P., & Tuffery, P. (2023). *Nucleic Acids Research, 51*, Article W432.
Roel-Touris, J., Bonvin, A. M. J. J., & Jiménez-García, B. (2020). *Bioinformatics, 36*, 950.
Roel-Touris, J., Jiménez-García, B., & Bonvin, A. M. J. J. (2020). *Nature Communications, 11*, 6210.
Roque-Borda, C. A., Saraiva, M. de M. S., Macedo Junior, W. D., Márquez Montesinos, J. C. E., Meneguin, A. B., Toledo Borges, A. B., Crusca Junior, E., Garrido, S. S., de Almeida, A. M., Marchetto, R., Chorilli, M., Berchieri Junior, A., Teixeira, S. R., Pavan, F. R., & Vicente, E. F. (2023). *Biomaterials, 293*, Article 121978.
Roque-Borda, C. A., Souza Saraiva, M. de M., Monte, D. F. M., Rodrigues Alves, L. B., de Almeida, A. M., Ferreira, T. S., de Lima, T. S., Benevides, V. P., Cabrera, J. M., Claire, S., Meneguin, A. B., Chorilli, M., Pavan, F. R., Junior, A. B., & Vicente, E. F. (2022). *ACS Infectious Diseases, 8*, 472.
Rostami, M., Ghorbani, M., Aman mohammadi, M., Delavar, M., Tabibiazar, M., & Ramezani, S. (2019a). *International Journal of Biological Macromolecules, 135*, 698.
Rostami, M., Ghorbani, M., Aman mohammadi, M., Delavar, M., Tabibiazar, M., & Ramezani, S. (2019b). *International Journal of Biological Macromolecules, 135*, 698.
Sales, L. S., Gimenes, M. da S., Meneguin, A. B., Barud, H. da S., Achcar, J. A., & Brighenti, F. L. (2023). *International Journal of Biological Macromolecules, 228*, 1.
Saponaro, A., Maione, V., Bonvin, A., & Cantini, F. (2020). *Biology Protocol, 10*.
Sato, H., & Feix, J. B. (2006). *Biochimica et Biophysica Acta (BBA) - Biomembranes, 1758*, 1245.
Seal, B. L., & Panitch, A. (2003). *Biomacromolecules, 4*, 1572.
Sekirov, I., & Finlay, B. B. (2009). *The Journal of Physiology, 587*, 4159.
Song, Y., Zhang, J., Zhu, L., Zhang, H., Wu, G., & Liu, T. (2024). *Food & Function, 15*, 8629.
Spósito, L., Fonseca, D., Gonçalves Carvalho, S., Sábio, R. M., Marena, G. D., Bauab, T. M., Bagliotti Meneguin, A., Parreira, P., Martins, M. C. L., & Chorilli, M. (2024). *European Journal of Pharmaceutics and Biopharmaceutics, 199*, Article 114280.
Stachowiak, N., Kowalonek, J., & Kozlowska, J. (2021). *Materials, 14*, 3044.
Sun, H., Hong, Y., Xi, Y., Zou, Y., Gao, J., & Du, J. (2018). *Biomacromolecules, 19*, 1701.
Sun, H., Li, Y., Tian, S., Xu, L., & Hou, T. (2014). *Physical Chemistry Chemical Physics, 16*, Article 16719.
Swanson, K., Walther, P., Leitz, J., Mukherjee, S., Wu, J. C., V Shivnaraine, R., & Zou, J. (2024). *Bioinformatics, 40*.
Tenland, E., Pochert, A., Krishnan, N., Umashankar Rao, K., Kalsum, S., Braun, K., Glegola-Madejska, I., Lerm, M., Robertson, B. D., Lindén, M., & Godaly, G. (2019). *PLoS One, 14*, Article e0212858.
Tian, B., & Liu, J. (2020). *Journal of the Science of Food and Agriculture, 100*, 1392.
Trovatti, E., Tang, H., Hajian, A., Meng, Q., Gandini, A., Berglund, L. A., & Zhou, Q. (2018). *Carbohydrate Polymers, 181*, 256.
Volić, M., Pajić-Lijaković, I., Djordjević, V., Knežević-Jugović, Z., Pećinar, I., Stevanović-Dajić, Z., Veljović, Đ., Hadnadjev, M., & Bugarski, B. (2018). *Carbohydrate Polymers, 200*, 15.
Wang, C.-K., Shih, L.-Y., & Chang, K. (2017). *Molecules, 22*, 2037.
Wang, X., Song, Z., Wei, S., Ji, G., Zheng, X., Fu, Z., & Cheng, J. (2021). *Biomaterials, 275*, Article 120913.
Wang, S., Wu, J., Tian, Y., & Zhou, S. (2024). *Science China Materials, 67*, 3763.
Wang, Y.-R., Yang, Q., Jiang, Y.-X., & Chen, H.-Q. (2024). *Food Hydrocolloids, 151*, Article 109798.
Wang, Y., Zhang, Y., Su, R., Wang, Y., & Qi, W. (2024). *Journal of Materials Chemistry B, 12*, 5061.
Wang, Y., Zhang, X., Wan, K., Zhou, N., Wei, G., & Su, Z. (2021). *Journal of Nanobiotechnology, 19*, 253.
Wegiel, L. A., Mauer, L. J., Edgar, K. J., & Taylor, L. S. (2013). *Journal of Pharmaceutical Sciences, 102*, 171.
Wen, Y., Chen, X., Yan, H., & Lin, Q. (2022). *Gels, 8*, 799.
Weng, G., Wang, E., Chen, F., Sun, H., Wang, Z., & Hou, T. (2019). *Physical Chemistry Chemical Physics, 21*, Article 10135.
Weng, G., Wang, E., Wang, Z., Liu, H., Zhu, F., Li, D., & Hou, T. (2019). *Nucleic Acids Research, 47*, Article W322.
Xun, X.-M., Zhang, Z.-A., Yuan, Z.-X., Tuhong, K., Yan, C.-H., Zhan, Y.-F., Kang, G.-P., Wu, Q.-Y., & Wang, J. (2023). *Sustainable Chemistry Pharmaceutical, 32*, Article 100974.
Yuan, X., Zhou, Y., Bi, J., Li, S., Wu, H., Zeng, M., Pan, Y., Lin, W., Zhou, M., Zhang, Z., Chen, A., & Wu, H. (2025). *International Journal of Biological Macromolecules, 306*, Article 141493.
Zhang, L., & Gallo, R. L. (2016). *Current Biology, 26*, R14.
Zhang, F., Khan, M. A., Cheng, H., & Liang, L. (2019). *Journal of Food Engineering, 247*, 9.
Zhang, Y.-Z., & Li, Y.-Y. (2014). *World Journal of Gastroenterology, 20*, 91.
Zhang, C., Liu, S., Zhu, Q., & Zhou, Y. (2005). *Journal of Medicinal Chemistry, 48*, 2325.
Zhang, W., Yu, X., Li, Y., Su, Z., Jandt, K. D., & Wei, G. (2018). *Progress in Polymer Science, 80*, 94.
Zheng, M., Zhang, W., & Lu, S. (2024). *International Journal of Biological Macromolecules, 263*, Article 130398.
Zhong, M., Sun, Y., Sun, Y., Fang, L., Wang, Q., Qi, B., & Li, Y. (2022). *Food Chemistry, 394*, Article 133514.